DEVELOPMENT OF DEVICE PROCESSING TECHNIQUES FOR III- NITRIDES

By

CATHERINE B. VARTULI

A DISSERTATION PRESENTED TO THE GRADUATE SCHOOL OF THE UNIVERSITY OF FLORIDA IN PARTIAL FULFILLMENT OF THE REQUIREMENTS FOR THE DEGREE OF DOCTOR OF PHILOSOPHY

UNIVERSITY OF FLORIDA

1996

In loving memory of my grandfather, Patrick Vartuli, Sr.

ACKNOWLEDGMENTS

I am very grateful for the guidance, advice and support of my advisor, S.J. Pearton. C.R. Abernathy, J.W. Lee, J.D. MacKenzie and the staff of the Microfabritech Facility have helped with the work done at the University of Florida. I am grateful to my committee members J.R. Childress, F. Sharifi and J. Simmons for their guidance. The work at University of Florida was supported by the National Science Foundation (DMR-9421109), an AASERT grant through ARO (Dr. J. M. Zavada), a DARPA grant (A. Husain) administered by Air Force Office of Scientific Reasearch (G.L. Witt), and a University Research Initiative grant #N00014-92-J-1895 administered by ONR.

At Sandia National Laboratories, the assistance of R.J. Shul, J.C. Zolper, M.L. Lovejoy, A.G. Baca and M. Hagerott-Crawford, as well as the technical help of J. Escobedo, M.A. Cavaliere, D. Tibbets, G.M. Lopez, A.T. Ongstad, J. Eng and P.G. Glarborg, is appreciated. The

work at Sandia was supported by Department of Energy contract DE-AC04-95AL85000.

The support and encouragement of my family and friends were indispensable, and are much appreciated. Special thanks is due to Lisa Kore for her support and assistance.

TABLE OF CONTENTS

LIST OF TABLES

LIST OF FIGURES

Abstract of Dissertation Presented to the Graduate School of the University of Florida in Partial Fulfillment of the Requirements for the Degree of Doctorate of Philosophy

DEVELOPMENT OF DEVICE PROCESSING TECHNIQUES FOR III- NITRIDES

By

Catherine B. Vartuli

December, 1996

Chairman: Dr. S.J. Pearton
Major Department: Materials Science and Engineering

Several new processing techniques needed to fabricate III-V nitride based photonic and electronic devices were developed. These processes include high temperature annealing, implant doping and isolation, wet and dry etching, and ohmic contact formation. As an example, heat treatments are necessary in many device processing steps. The surface stability of AlN, GaN, InN, InAlN and InGaN was examined under rapid thermal annealing conditions, and the results compared to the theoretical vapor curves. The preferential loss of N from the surface is the most significant surface degradation mechanism. Next, the ion implantation isolation and doping of GaN, with N^+ (isolation), Si

(n-type doping) and Mg^+/P^+ (p-type doping) was examined. Isolation implantation was also studied in InAlN and InGaN using N^+ ions. After implantation for doping, samples were annealed at various temperatures to activate the ions. The electrical characteristics were measured as a function of anneal and measurement temperature to obtain the percent activation and the ionization energy levels of the implanted ions. The excellent chemical stability that makes these III-nitrides attractive for high temperature devices also makes it difficult to develop etching techniques for device fabrication. Wet chemical etching of AlN and $In_xAl_{1-x}N$ in KOH based solutions was examined as a function of etch temperature, crystal quality and In composition. Dry etching of the nitrides was investigated under Electron Cyclotron Resonance (ECR) and Reactive Ion Etching (RIE) conditions in Cl_2/Ar and $CH_4/H_2/Ar$ discharges, and in ECR in ICl/Ar and IBr/Ar plasmas. The fastest etch rates yet reported for GaN, InGaN and InN were achieved under ECR conditions in ICl/Ar chemistries. AlGaN etch rates were determined in BCl_3/Ar and Cl_2/Ar plasmas as a function of AlN composition, rf and microwave power. Etch selectivities were calculated for GaN over InN, InAlN, InGaN and AlN. Finally, ohmic contacts were formed on InN, InAlN and

InGaN with W, WSi_x and Ti/Al metalization schemes. The contacts were annealed at various temperatures, and the specific contact resistance measured. Low resistance contacts were formed in most cases. Temperature-dependent transmission line measurements showed that field emission of electrons was the dominant conduction mechanism.

CHAPTER 1

INTRODUCTION

Wide bandgap semiconductors such as SiC, the II-VI systems (ZnS, ZnSe, CdTe) and the III-V nitrides (GaN, AlN, InN) are being investigated for use in short-wavelength photonics and high temperature electronics.[1-15] The development of these materials has been hampered by a lack of lattice matched substrates for epitaxial growth, poor patterning techniques, relatively poor ohmic contact technology and an inability to control native defect populations. The advances made recently in these areas have made possible a number of devices fabricated from wide band gap semiconductors.

The InGaN/AlGaN heterostructure is attracting tremendous interest for use in blue/UV lasers, and light emitting diodes, as well as high temperature electronics. GaN[16] and double-heterostructure InGaN/GaN[2] and AlGaN/GaN[17] blue and green light-emitting diodes (LEDs) are commercially available. They are being used extensively (production of InGaN/GaN LEDs is now 10^7 devices per month at Nichia Chemical) in full color displays and for traffic lights in the Tokyo area. Nakamura et al. recently reported a InGaN/AlGaN laser,[16] and later Toshiba announced a GaN-based

laser,[21] Further work has been reported on laser design[22] and LED reliabilty.[23] Metal semiconducting field effect transistors (MESFETs),[24,25] junction FET's (JFET's),[26] and AlGaN/GaN heterostructure FET's (HFET's)[16-32] have also been developed in recent times.

Wide bandgap binaries such as GaN (3.4 eV) and AlN (6.2 eV) may also find application in passivation of semiconductor surfaces because of their chemical inertness and excellent mechanical properties. [12]

Current drawbacks to more widespread applications of these materials include lack of etching techniques, both wet and dry, and lack of implant doping and isolation methods, as well as low resistance ohmic contacts. The III-V nitrides are chemically very inert and therefore resist chemical attack by conventional acids. This has made it difficult to develop processing steps for these materials, and their wide band gaps make it hard to form ohmic contacts.

As can be seen in Fig. 1, a large number of processing modules are needed to produce a device. Implantation isolation is used to electrically or optically isolate the device and still maintain planarity. N- and p-type doping are used to form low resistance contact regions. Thermal activation of the implants and alloying of the contacts is necessary, and patterning of the material by both wet and dry etching is required.

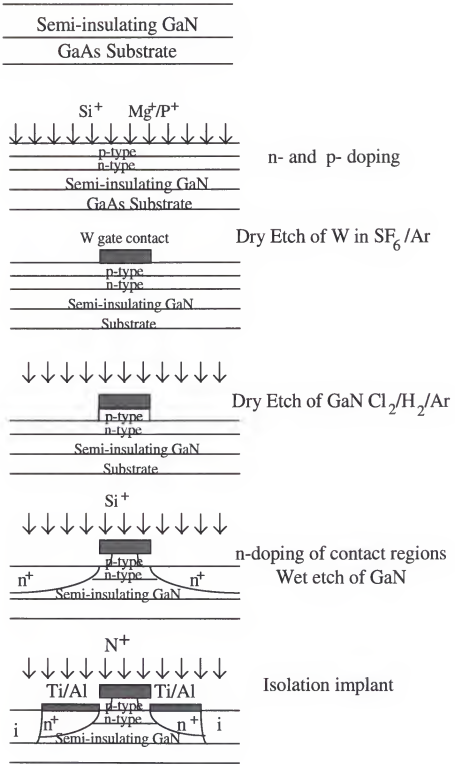

Figure 1. Processing steps for a GaN-based device.

This thesis involves investigation of the various processing techniques needed to develop high performance, reliable III-V nitride based photonic and electronic devices. A summary of the results of this development is given in Table I. Many of the processing steps require high temperature annealing, including maximization of the resistance of implant isolated regions, activation of implanted ions or high temperature alloying of metal contacts. Ensuring that surface degradation of the III-V nitrides does not occur during these high temperature anneals is critical to device performance. The surface stability of AlN, GaN, InN, InAlN and InGaN was examined under rapid thermal annealing conditions, and the results compared to theoretical vapor curves. The preferential loss of N from the surface is the most significant surface degradation mechanism.

A process was also developed for forming semi-insulating regions in initially n- or p-type GaN using multiple energy N^+ implantation, and in $In_xAl_{1-x}N$ and $In_xGa_{1-x}N$ implanted with multiple energy N^+ ions and subsequently annealed up to 900 °C. Variable temperature Hall measurements were used to obtain the energy level of the defects controlling conduction after different implantation and annealing steps. Sheet

Table I. Summary of results.

Process	AlN	GaN	InN	InGaN	InAlN
Capless Annealing (Thermal Surface Stability)	> 1000 °C	1000 °C	600 °C	800 °C	800 °C
Implant isolation		> 10^9 $\Omega \bullet cm^2$ with N^+ anneal to 750 °C		problema-tic	~10^9 $\Omega \bullet cm^2$ with N^+ anneal to 650 °C
Doping		N-type (Si^+) p-type (Mg^+/P^+) anneal to 1100 °C			
Wet Etching	KOH-based solution	No etch	No etch	No etch	KOH-based solution
Dry etching (ECR)	0.22μm/min	1.3 μm/min	1.1μm/min	0.7μm/min	0.28 μm/min
Ohmic Contacts (W-based)			~$10^{-7}\Omega \bullet cm^2$	~$10^{-7}\Omega \bullet cm^2$	~10^{-4} $\Omega \bullet cm^2$

resistances of $\geq 5\times10^{9}$ $\Omega/\square$ for N^{+} implanted GaN, and $> 10^{8}$ $\Omega/$ were obtained for N^{+} implanted InAlN. In InGaN, sheet resistances typically 50-100 times higher than the as-grown values were obtained using the N^{+} implantation. In addition, n- and p-type doping of ion implanted species in GaN was obtained. Carrier activation percentages were obtained of 93% for Si (which created n-type GaN) and 62% for Mg, which when co-implanted with P^{+} produced p-type GaN.

Dry etching of the nitrides was investigated under Electron Cyclotron Resonance (ECR) and Reactive Ion Etching (RIE) conditions in Cl_2/Ar and $CH_4/H_2/Ar$ discharges. A comparison was made of RIE and ECR etching of GaN, AlN, InN and InGaN in Cl_2/Ar and $CH_4/H_2/Ar$ plasmas using the same reactor and etch conditions. Etch rates up to an order of magnitude faster were measured under ECR conditions. In addition, ECR etching of GaN, InN, InAlN, AlN and InGaN in ICl/Ar and IBr/Ar plasmas was examined under various plasma compositions, microwave powers and rf powers. The GaN, InN and InGaN etch rates reached ~ 13000 Å/min, 11500 Å/min and ~7000 Å/min, respectively, at 250 W rf and 1000 W microwave power in ICl/Ar plasma discharges. These are the fastest yet reported for these materials. The etched surface of GaN was found to be smooth with no significant loss of N from the surface at low rf powers. Etch selectivities were calculated

for these chemistries for InN, InAlN, InGaN or AlN with respect to GaN.

Wet chemical etching of AlN and $In_xAl_{1-x}N$ in KOH based solutions was studied as a function of etch temperature, crystal quality and In composition. Both AlN and InAlN samples showed an increase in etch rates with solution temperature. The rate limiting step was diffusion of ths reactant species to the nitride surface. A maximum occured in the etch rate of InAlN at ~ 36 % InN, presumably due to competing mechanisms between decreasing bond strength and decreasing chemical reactivity with increasing InN composition.

Finally, ohmic contacts were formed on InN, InAlN and InGaN with W, WSi_x and Ti/Al. The contacts were annealed at various temperatures, and the specific contact resistance measured. W, WSi_x and Ti/Al were found to produce low resistance ohmic contacts on n^+ InGaN and InN. W contacts proved to be the most stable, and also gave the lowest resistance on InGaN and InN, $\rho_c < 10^{-7}\ \Omega\cdot cm^2$ after 600 °C anneal, and $1x10^{-7}\ \Omega\cdot cm^2$ after 400 °C anneal, respectively. The predominant conduction mechanism was found to be field emission for InN and InGaN samples.

The GaN, AlN, InN, InGaN and InAlN samples used in these studies were grown using Metal Organic Molecular Beam Epitaxy (MO-MBE) on semi-insulating, (100) GaAs substrates

or Al_2O_3 c-plane substrates in an Intevac Gen II system.[33,34] The group-III sources were triethylgallium, trimethylamine alane and trimethylindium, respectively, and the atomic nitrogen was derived from an ECR Wavemat source operating at 200 W forward power. The layers were single crystal with a high density (10^{11}-10^{12} cm^{-2}) of stacking faults and microtwins. The GaN and AlN were resistive as-grown, (~$10^{9}\Omega$·cm for GaN and ~$10^{11}\Omega$·cm for AlN) and the InN was highly autodoped n-type (>10^{20} cm^{-3} with 300 K mobility of ~1-100 $cm^{2}\cdot V^{-1}\cdot s^{-1}$) due to the presence of native defects. InAlN and InGaN were found to contain both hexagonal and cubic forms. The InAlN and InGaN were conducting n-type as grown due to residual autodoping by native defects. These characteristics are quite typical for nitrides currently available.[35-39]

CHAPTER 2

SURFACE DEGRADATION

Introduction

High temperature annealing is necessary in many of the processing steps for GaN-based devices, including maximization of the resistance of implant isolated regions,[40,41] activation of implanted ions[42] or high temperature alloying of metal contacts.[36,37,43,44] A key issue is the question of surface degradation of the III-V nitrides during these high temperature anneals. A variety of authors previously published experimental and theoretical vapor pressure curves for AlN,[45-48] GaN[49-51] and InN.[38,52-54]

In all of this previous work the equilibrium N_2 pressures above the solid (or solid plus liquid) have been the focus. In many process steps, rapid thermal annealing (RTA) using the proximity geometry is employed, which is a non-equilibrium situation. In this case the sample is placed face-down on a substrate that can provide a group V partial pressure, and heating by tungsten-halogen lamps produces temperature ramp rates of 100 - 200 $°C \bullet s^{-1}$. Zolper et al.[55] observed that the luminescence and surface morphologies of GaN annealed in flowing N_2 actually improved for RTA

temperatures up to 1100 °C. Similar results were obtained at lower temperatures by Lin et al.[39] This is a common situation for lattice-mismatched systems (e.g. GaAs/Si), where post-growth or even in-situ annealing is generally found to improve structural and optical properties, provided that group V loss from the surface can be suppressed and that external impurities do not diffuse in during the anneal.

EXPERIMENTAL

The GaN, AlN, InN, InGaN and InAlN samples used were primarily grown on Al_2O_3 in this study, because they can be annealed to higher temperatures than those grown on GaAs without worrying about backside degradation. In the cases where both kinds of samples were used (i.e. annealing temperatures below ~900°C), no significant differences were observed in the thermal stability of the nitrides. The GaN and AlN were resistive as-grown, (~$10^9\Omega$·cm for GaN and ~$10^{11}\Omega$·cm for AlN), the InN was highly autodoped n-type (>10^{20} cm^{-3}) and the $In_{0.75}Al_{0.25}N$ and $In_{0.5}Ga_{0.5}N$ were conducting n-type as-grown (~ 10^{19} cm^{-3}).

The samples were annealed in a rapid thermal anneal (RTA) system (AG 410T) face down on a GaAs substrate for 10 s at temperatures between 650 - 1150 °C in a N_2 atmosphere. GaAs was employed in the hope that decomposition of As from

these substrates might help to prevent nitrogen loss from the nitride samples.[56] The presence of a group V overpressure, even if it is not the same element as the group V component of the substrate, is generally found to help preserve III-V substrates. The sheet resistance was measured at room temperature on a Van der Pauw Hall system with InHg alloyed contacts (300 °C, 3 min) on the corners. An Atomic Force Microscope (AFM), operated in tapping mode with Si tips, was used to measure the root mean square (RMS) roughness of the samples. The surface morphology was also examined with a scanning electron microscope (SEM). Energy dispersive X-ray spectrometry (EDAX) was used to analyze the surface composition of some annealed InAlN samples. Auger Electron Spectroscopy (AES) was used to investigate near-surface stoichiometry before and after annealing.

RESULTS AND DISCUSSION

The sheet resistance normalized to the as-grown value for all of the nitride samples is shown in Fig. 2 as a function of annealing temperature. The values for the GaN, AlN and InN are found to drop by approximately three orders of magnitude with annealing, up to 900 °C. The binary material becomes strongly n-type in all cases. The sheet resistance for AlN continues drop steadily with anneal

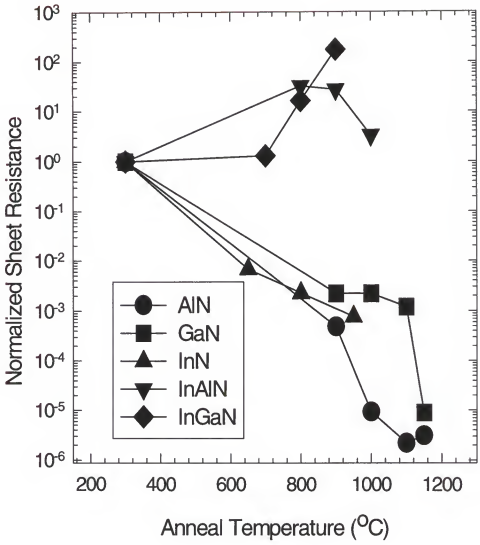

Figure 2. Sheet resistance normalized to the as-grown value for AlN, GaN, InN, InAlN and InGaN as a function of annealing temperature. The initial sheet resistances were ~10^8ohm per square (AlN), 10^6 ohm per square (GaN), 1.6x10^5ohm per square (InN) and 10^6ohm per square (InAlN and InGaN).

temperature until 1100 °C. As will be shown below, AlN shows only a small loss of N from the surface as determined by AES. However, the electrical measurements are more sensitive to small changes in the composition than the Auger. Here it is believed that the N vacancies created by the loss of N from the surface are creating shallow donors. This agrees with the theoretical prediction of Maruska and Tietjen.[57] The actual values of sheet resistance for AlN are much higher than the GaN up to 900 °C, and significantly higher than InN at all temperatures. The data in Figure 2 is in agreement with the trends predicted for the melting points and vapor pressures for these materials. AlN is predicted to have some stablity under N_2 gas up to ~2500 °C,[9] and to melt at ~ 3700 °C at atmospheric pressure.[11] GaN is predicted to melt at ~3000 °C[11] and InN at only ~2400 °C[11] and to degrade at 600 °C.[8] AES has confirmed loss of N from the annealed GaN sample which would suggest that N vacancies are contributing to the conductivity. Above 900 °C Ga vacancies in the GaN may also be creating compensating shallow acceptors. Ga or N antisite defects, which form deeper traps, might also be formed, but there was no evidence of additional compensation in the electrical measurements. At 1150 °C the sheet resistance for the GaN drops sharply indicating that N is being lost at a much greater rate than

the Ga. Groh et al.[58] showed loss of nitrogen beginning at 710 °C in vacuum annealed GaN, with significant loss at ≥ 980 °C. The sheet resistance for the InN drops steadily over the temperature range, which correlates to the problems of avoiding non-stoichiometry in annealed InN. The large size difference between the N and In make this material less stable during heating.

The sheet resistance for both InGaN and InAlN, on the other hand, increases with annealing. The InAlN sheet resistance increases by a factor of 10^2 from the value for the as-grown material when annealed at 800 °C. Its resistance then remains constant to 900 °C, and then decreases slightly at 1000 °C. For InGaN the sheet resistance remains constant up to 700 °C and then increases rapidly with increasing temperature. This suggests that simple N vacancies are not the cause of the residual n-type conductivity in these samples since at the highest temperatures N was lost from the surface, as described below. However, these samples become less conducting, suggesting creation of compensating acceptors or annealing of the native donors is occurring. It is likely, in contrast to the binary nitrides, that the V_N have several different energy levels in the ternaries because of the differences in strength between In-N and Ga-N bonds. Some of these may be

creating a deep acceptor which compensates the shallow donors, or a deep level electron trap, making the material more resistive. There could also be the presence of compensating V_{Ga} or V_{In}-related defects, which might be easier to form in ternaries because of different sizes and bond strengths of the In and Ga. Finally, it is possible that at least some of the conductivity in the ternaries is due to carbon-related donors,[59] and subsequent annealing might produce carbon self-compensation, as in other III-V's. At this point it is not possible to be more precise regarding the differences between the binaries and the ternaries and this is under close examination.

The RMS data normalized to the as-grown roughness as a function of anneal temperature is shown in Fig. 3 for AlN, GaN and InN. The AlN is still smooth at 900 °C, but becomes quite rough at 1000°C. Further surface reconstruction continues at higher annealing temperatures. At 1150 °C the sample becomes smooth again- in fact slightly smoother than the as-grown sample. GaN shows no roughening, becoming smoother with annealing due to defect annealing and surface reconstruction. InN, on the other hand, is already a factor of two rougher than for as-grown samples at 650 °C, indicating the weaker bond strength of this material. The individual AFM scans are shown in Fig. 4 for AlN and GaN and in Fig. 5 for InN.

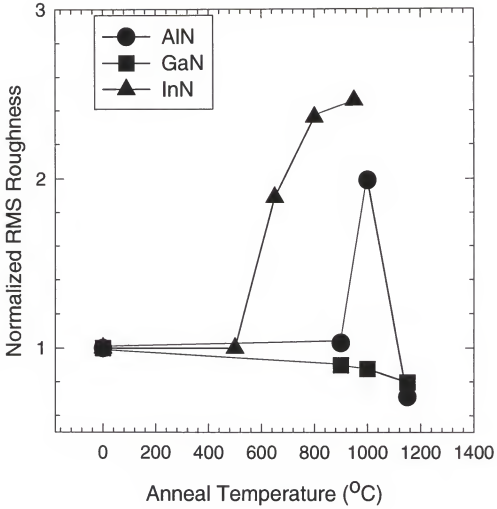

Figure 3. The RMS data normalized to the as-grown roughness as a function of anneal temperature for AlN, GaN and InN. The initial rms values were 4nm (AlN), 8.9nm (GaN) and 16.1nm(InN).

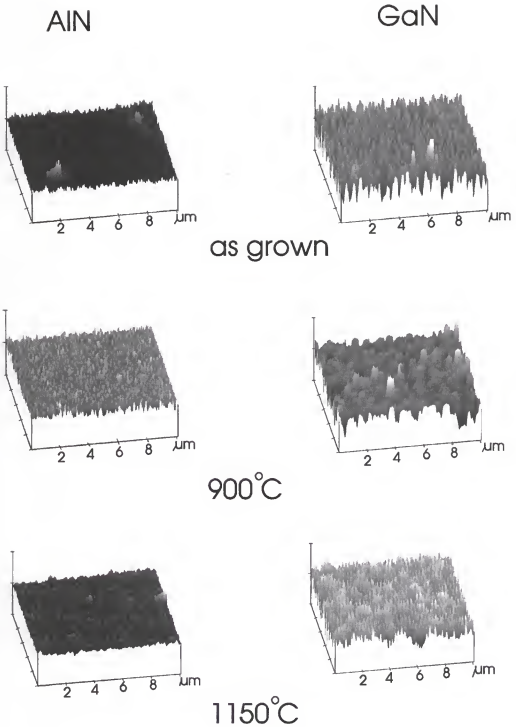

Figure 4. Individual AFM scans for AlN and GaN. Vertical scale is 100 nm per division.

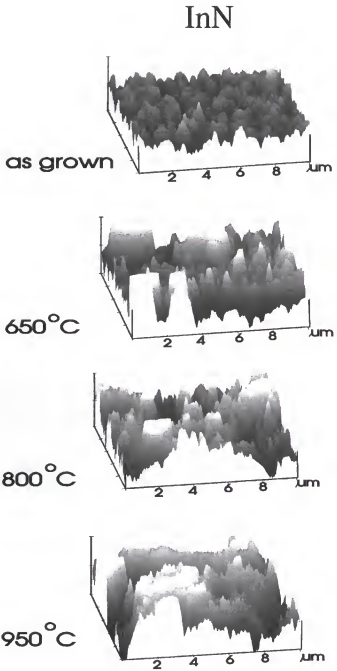

Figure 5. Individual AFM scans for InN. Vertical scale is 100 nm per division.

In Fig. 6 the RMS roughness for InAlN and InGaN are shown as a function of rapid thermal anneal temperature. It can be seen that the InAlN remained smooth until 800 °C, and at 900 °C has increased an order of magnitude in roughness. At 1000 °C the RMS roughness returns to a value close to that of the value for the as-grown material. This was found to be a result of In droplets forming on the surface for temperatures above 800 °C and then evaporating above 900 °C. The InGaN surface roughness was unchanged by annealing at 700 °C, with the roughness increasing above that temperature. In Fig. 7 the individual AFM scans are shown for the ternaries annealed at different temperatures. The surface of the samples became coarser above 800 °C, with large droplets forming. In the case of InAlN these droplets are removed by annealing at 1000 °C, where the surface evaporation is more congruent.

In Fig. 8 SEM pictures of AlN, GaN and InN are shown for as-grown, (left) and annealed (right) samples. AlN has no visible surface degradation, even at 1150 °C. GaN has become slightly rough and pitted at 1000 °C, and the InN surface has degraded badly at 800 °C, showing pits and various defect structures. InAlN is shown in Fig 9 for as-

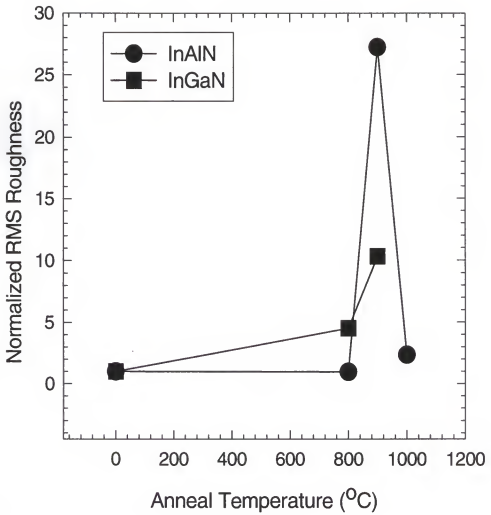

Figure 6. The RMS data normalized to the as-grown roughness as a function of anneal temperature for InAlN and InGaN. The initial rms values were 19.1nm (InAlN) and 23.2 nm (InGaN).

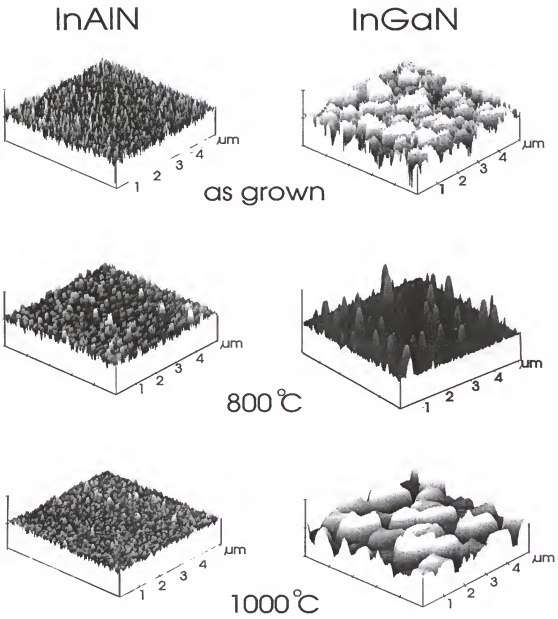

Figure 7. Individual ASM scans of InAlN and InGaN. Vertical scales is 100 nm per division.

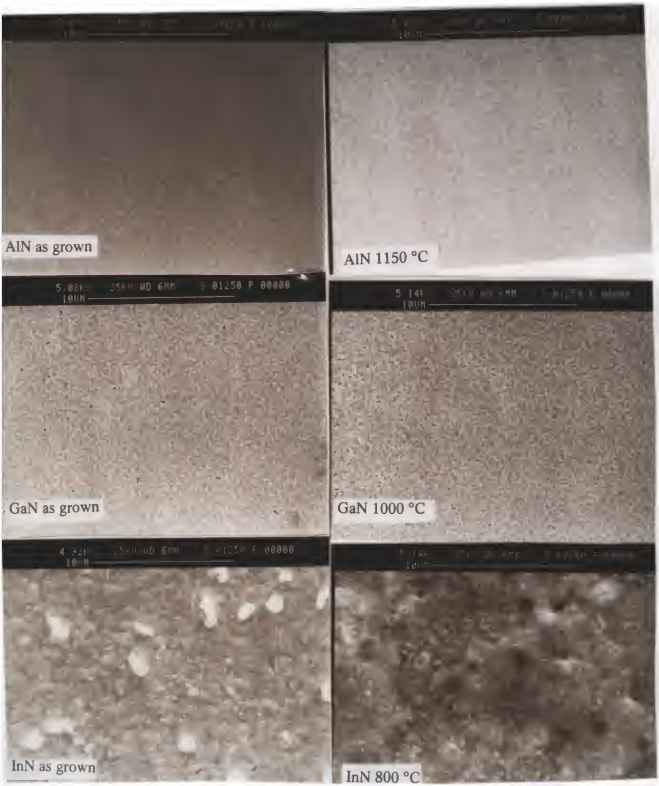

Figure 8. SEM micrographs of AlN, GaN and InN for as-grown, (left) and annealed (right) at the lowest temperature that shows significant visible degradation.

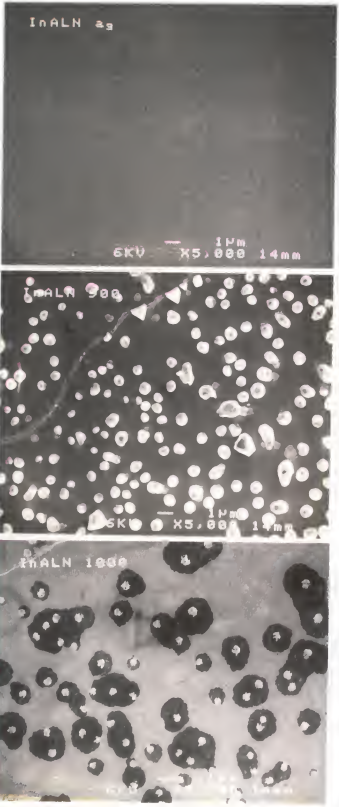

Figure 9. SEM micrographs of InAlN for as-grown (top), 900 °C anneal (middle) and 1000 °C anneal (bottom).

The unannealed surface is reasonably smooth with small particulates. At 900 °C In droplets are seen to form on the surface as determined by EDAX. At 1000 °C the In evaporated off the surface, leaving dark, In-deficient areas. This accounts for the reduced RMS roughness of the 1000 °C annealed sample. In droplets began to form on the surface of the InGaN samples at 800 °C and continue to grow at 900 °C. Confirmation that these are indeed In droplets comes from direct chemical identification by EDAX which showed a reduced Ga/In ratio around the precipitate relative to the background on which the precipitate sits.

In Figs. 10 through 12 the AES depth profiles and surface scans for AlN and GaN, as-grown and annealed at 1150 °C are shown. On all the samples the surface was contaminated with oxygen from a native oxide and adventitious carbon because of exposure to ambient when transferring the material from the annealing furnace to the AES analysis chamber. After the 1150 °C anneal of AlN (Fig. 10), less C, O and Al are found on the surface compared to the as-grown sample. Ga was found to have diffused into the top 50 Å of the material from the proximity wafer used during annealing. The N appears to have been lost only from the top 100 Å or so from the surface as a result of

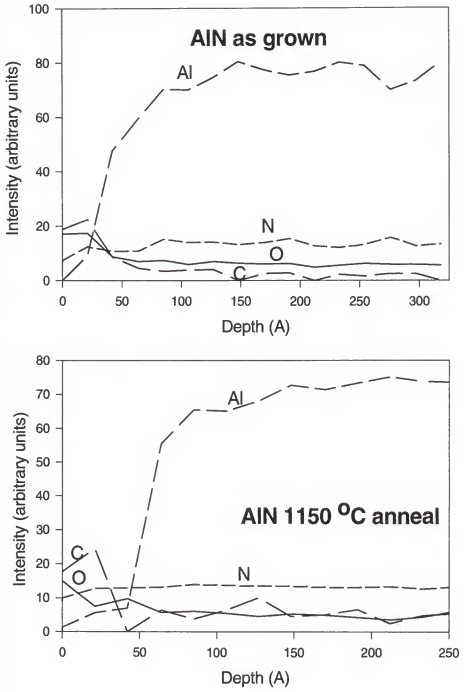

Figure 10. AES depth profiles for AlN as-grown and annealed at 1150 °C.

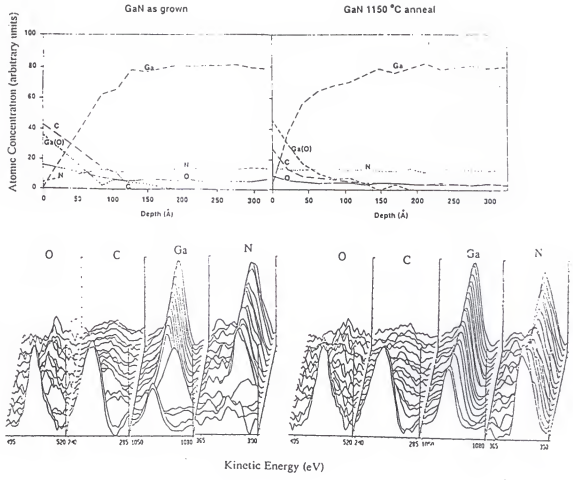

Figure 11. AES depth profiles for GaN as-grown and annealed at 1150 °C.

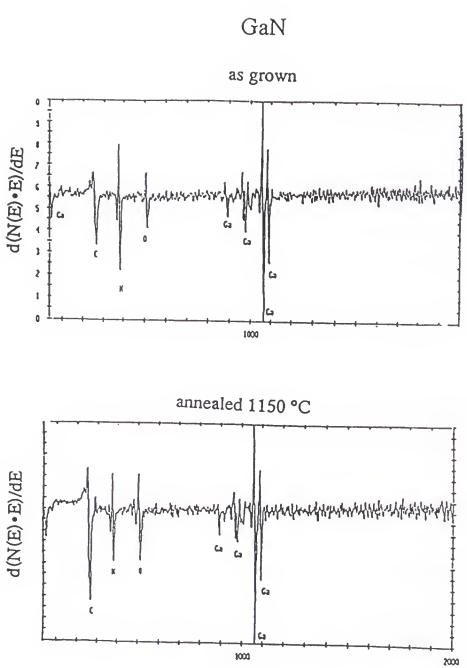

Figure 12. AES surface scans for GaN as-grown and annealed at 1150 °C.

annealing, showing the excellent thermal stability of this material.

For GaN (Fig. 11 and 12) the oxygen at the surface of the annealed sample has decreased, but the C content of the surface has increased, as has that of the Ga and N. The proximity cap worked well for the Ga component. The Ga/N ratio measured by raw AES counts increased from 1.73 on the as-grown samples to 2.34 after 1150 °C annealing, indicating that nitrogen was indeed lost from the surface. Similar data is shown in Fig. 13 and 14 for InAlN and InGaN as-grown and annealed at 1000 °C and 800 °C, respectively. Both materials show a definite decrease in the amount of N at the surface of the samples after anneal. In the case of InGaN there was also a reduction in In, which could be related to the changes in the electrical properties. For InAlN the amount of Al increased at the surface, and both samples experienced Ga diffusion in the first 50 Å or so from the proximity cap. The surfaces of all the samples show a loss of N, consistent with the SEM, AFM and EDAX results discussed above.

Conclusion

The III-V nitrides are thermally stable to relatively high temperatures. AlN and GaN remain smooth and stochiometric at 1000 °C, InAlN and InGaN up to 800 °C, and InN up to 600 °C. Above these temperature capping is

necessary to prevent the loss of N and, sometimes, In. Consistent with the predicted melting temperatures and thermal stabilities of the nitrides, it was found AlN to be somewhat more stable than GaN, and much more stable than InN. InAlN was found to be more stable than InGaN, as expected from a consideration of the binary component N_2 vapor pressures. AlN may prove to be a good capping material for the other nitrides, because of its high stability and the fact that it can be selectively removed by wet etching in KOH based solutions.[60]

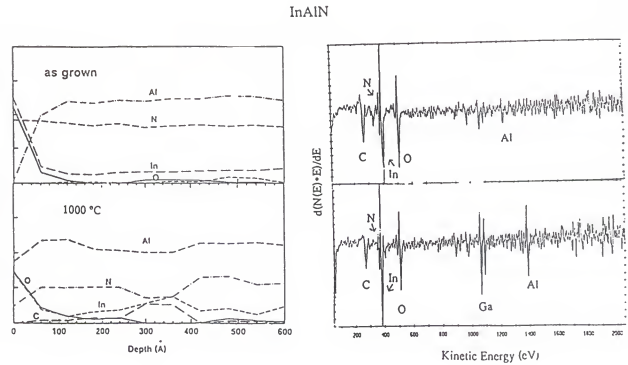

Figure 13. AES surface scans and depth profiles for InAlN as-grown and annealed at 1000°C.

InGaN

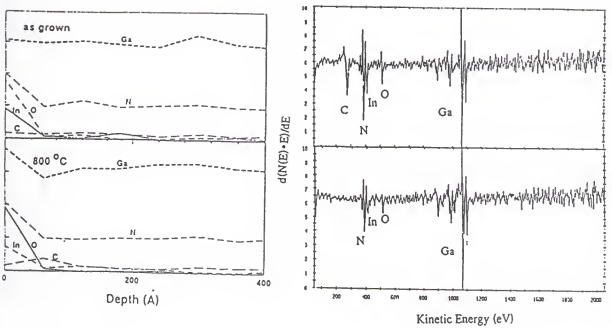

Figure 14. AES surface scans and depth profiles for InGaN as-grown and annealed at 800°C.

CHAPTER 3

IMPLANT ISOLATION AND DOPING

Introduction

Many of the recent advances in the III-nitrides have been made possible by the achievement of controlled n-type,[61,62] and for optical applications, p-type doping[10,16,63-68] during epitaxial crystal growth. The use of ion implantation for selective area doping or isolation is a critical requirement for advancement of GaN device technology. Generally implantation has been used to introduce impurities for study of their optical properties.[69] Maruska and Tiefjen have shown that GaN light-emitting diodes emit at 430 nm (violet) when implanted with Mg and at 590 nm (yellow) when co-implanted with Mg and Zn.[70] The use of Zn doping alone produced green emission. In these cases the implanted impurities behave as color centers. Wilson et al.[71] reported the observation of 1.54 μm luminescence of optically excited Er^{3+} in implanted GaN in which the Er was co-implanted with O. Diffusion studies of implanted dopants have shown there is no measurable redistribution of any species except S in GaN.[72] Implantation with either H^+ or He^+ ions was used for isolation in the transistors reported by Binari et al.,[34,73]

and creation of high resistance regions in $In_xGa_{1-x}N$ by N^+ or F^+ implantation has also been achieved.[41,74] The only report of electrical activation of a dopant species implanted in GaN involved Mg^+, with subsequent annealing at 800 °C.[7]

Ion Implantation Isolation Of GaN

A process was developed for the creation of semi-insulating ($\geq 5\times10^9$ $\Omega/\square$) regions in initially n- or p-type material using multiple energy N^+ implantation and subsequent annealing. This process is directly applicable to the fabrication of all-implanted metal-semiconductor field effect transistors (MESFETs), as well as other electronic and photonic devices.

The starting GaN epilayers were specifically doped n-type with Si (from a disilane source) or p-type with Mg (from biscyclopentadienyl magnesium), to levels in the range $4x10^{17}$- $4x10^{18}$ cm^{-3}. These were used for the isolation experiments. These intentionally doped wafers were implanted with $^{14}N^+$ at multiple energies of 50-250 keV and doses of 2-$6x10^{13}$ cm^{-2} to yield an approximately uniform N concentration of $2x10^{18}$ cm^{-3} throughout the doped GaN. The samples were subsequently annealed between 400-950°C, for 10 sec in the same AG Associates 410T system. and electrical characterization was performed by Van der Paww Hall measurements.

Figure 15 shows the evolution with annealing temperature of the sheet resistance of initially n- or p-type GaN implanted with a multiple energy N^+ scheme. As observed with more conventional III-V materials, the sheet resistance actually increases with annealing temperature up to ~ 750 °C, and decreases thereafter. This is usually ascribed to the introduction of deep level traps in the material by the implantation damage which compensates the initial conductivity.[19] Annealing up to a specific temperature (which depends on ion dose and species) reduces carrier hopping and produces an increase in sheet resistance, but beyond that temperature the deep levels are removed and the conductivity of the material increases. A similar behavior appears operative in both n- and p-type GaN implanted with N^+. Note that the maximum sheet resistances obtained ($>5x10^9$ Ω/ in both conductivity types) are higher than reported for lower bandgap materials such as GaAs and GaP.[75]

An estimate of the energy level of the main defect controlling the conductivity of the implanted GaN can

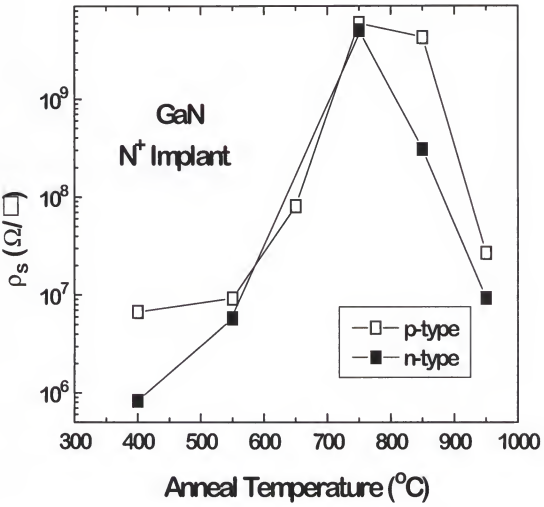

Figure 15. Sheet resistance as a function of annealing temperature for N^+ implanted n- or p-type GaN.

be obtained from the Arrhenius plot of the temperature dependence of the sample sheet resistance. Figure 16 shows this type of analysis for both n- and p-type GaN implanted with the multiple energy N^+ isolation scheme, and then annealed at 750 °C, where the sheet resistance is maximized. The activation energy for the p-type sample is 0.90 eV, and that for the n-type material is 0.83 eV. These energy values represent the approximate position of the Fermi level and show why very high resistances can be obtained in implant-isolated GaN. However, an optimum situation is to produce midgap levels in isolated material i.e., at ~ 1.6 eV in GaN. The microstructural nature of the defects responsible for the carrier compensation is not known at this point, as indeed is the situation for all III-V semiconductors, but is likely to consist of native defect (vacancy and/or interstitial) complexes. In both n- and p-type GaN these complexes anneal out above ~ 750°C.

In summary, high resistivity regions can be created in initially doped GaN by N^+ implantation. Subsequent annealing achieves sheet resistances above $5x10^9$ $\Omega/$ in both n- and p-type material.

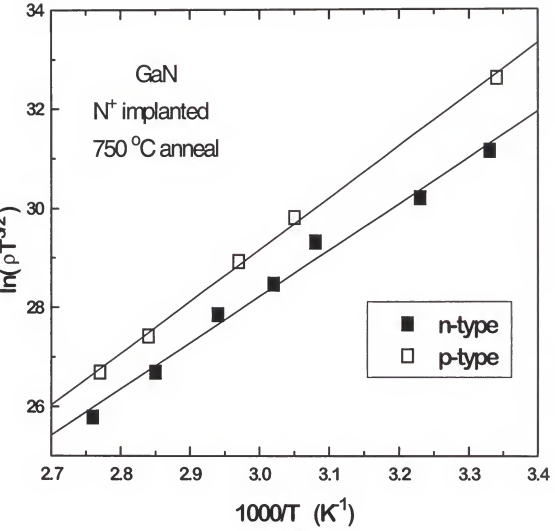

Figure 16. Arrhenius plot of sheet resistance of N^+ implanted n- and p-type GaN annealed at 750 °C.

Ion Implantation Isolation Of InAlN And InGaN

An investigation into the implant isolation characteristics of $In_xAl_{1-x}N$ and $In_xGa_{1-x}N$ was made. $In_xAl_{1-x}N$ (x = 0.75) or $In_xGa_{1-x}N$ (x = 0.33-1) were implanted with ^{14}N ions at multiple energies in the range 40 - 270 keV to produce a uniform ion and damage profile throughout the film thickness. Three different dose ranges were investigated, namely $5x10^{12}$ cm^{-2} (low dose), $5x10^{13}$ cm^{-2} (medium dose) and $5x10^{14}$ cm^{-2} (high dose). These refer to the doses for the lowest energy implant (40 keV). For the higher energies the doses were adjusted to keep a constant peak ion concentration. Post-implant annealing was carried out for 30 secs at temperatures between 150-900 °C in an AET rapid thermal furnace with the samples contained in a SiC-coated graphite susceptor. Hall measurements were performed using evaporated Pd/Au contacts at the corners of the 5x5 mm^2 samples.

Figure 17 shows the sheet resistance as a function of anneal temperature for N^+ implanted $In_{0.75}Al_{0.25}N$. The sheet resistance increases up to ~ 600 °C, and then is reduced to the original unimplanted values at ~ 800 °C. This behavior is typical of that seen in other implanted III-V semiconductors,[74] and is caused by the introduction of deep acceptor states related to the

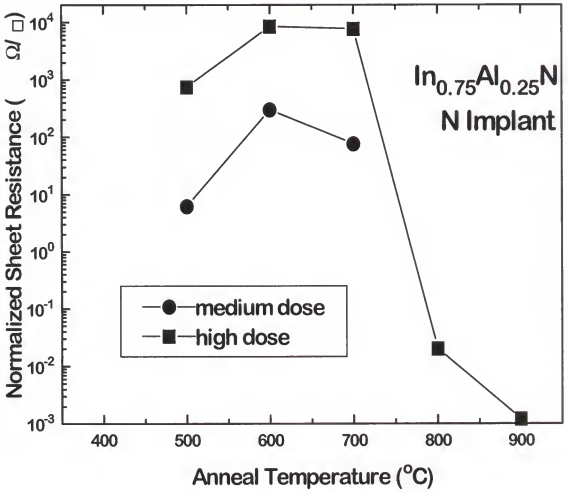

Figure 17. Normalized sheet resistance ratios versus anneal temperature for $In_{0.75}Al_{0.25}N$ implanted with different doses of N^+ at multiple energies.

implant damage that compensate the shallow native donors. This produces an increase in sheet resistance of the material, the magnitude of which is dose-dependent. The usual situation is that all of the shallow levels are compensated but some residual conductivity remains due to the presence of intra-defect hopping of trapped carriers from one closely-spaced trap site to another.[76-79] In other words there is an excess of deep states over that required for optimum compensation. Subsequent annealing removes these excess states, leading to an increase in sheet resistance of the material. Continued annealing above ~600 °C for $In_{0.75}Al_{0.25}N$ reduces the deep acceptor concentration below that required to trap all of the original free electrons, and the conductivity increases back to the pre-implanted value. In the present case, annealing above 800 °C actually produces a sheet resistance lower than in the as-grown samples due either to loss of nitrogen from the uncapped material or the existence of additional shallow donor states created by the implantation.[20] This leads to the conclusion that nitrogen does not produce chemical deep states in InAlN or the high resistance values would be maintained even at the maximum annealing temperatures. Nitrogen is known to create chemical deep levels in AlGaAs.[16,79,80] Note that even in this relatively conducting InAlN, implantation and optimized annealing is capable of producing increases in

sheet resistance of 3-8x10^3 times (absolute values > 10^8 Ω/). This is well above the values required for electronic device isolation ($\geq 10^6$ Ω/).[20]

Temperature dependent measurements of the sheet resistance of an $In_{0.75}Al_{0.25}N$ sample implanted with either a medium or high dose of N^+ ions and annealed at 600 °C are shown in Figure 18. The activation energy obtained for the medium dose sample is ~ 0.19 eV, consistent with its lower sheet resistance relative to that of the higher dose material where the activation energy was 0.54 eV. Note that for optimum implant isolation it is desirable to create mid-gap states. In InAlN the states created are still relatively high in its bandgap, similar to the behavior of InP and InGaAs.[20,22,23]

Turning to $In_xGa_{1-x}N$, Figure 19 shows the increase in sheet resistance of N^+ implanted material of three different compositions, as a function of annealing temperature. The maximum increases in sheet resistance are less than a factor of 10^3. Once again there is no evidence for a chemically active deep acceptor state for nitrogen. In this highly conducting $In_xGa_{1-x}N$ the absolute sheet resistances achievable are borderline for electronic device isolation, but are acceptable for applications such as current path delineation in photonic devices.

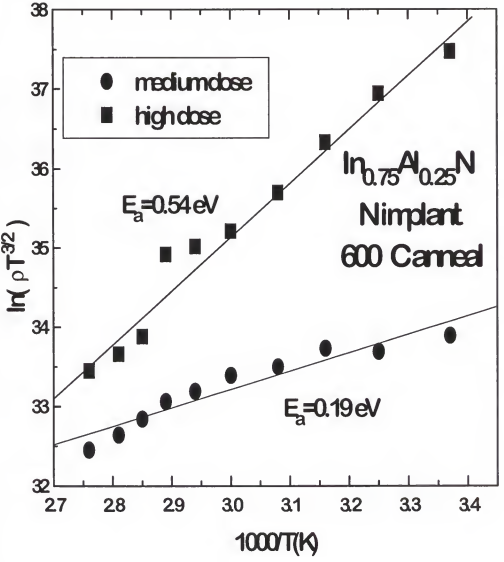

Figure 18. Arrhenius plots of sheet resistance of N^+ implanted $In_{0.75}Al_{0.25}N$ after annealing at 600 °C.

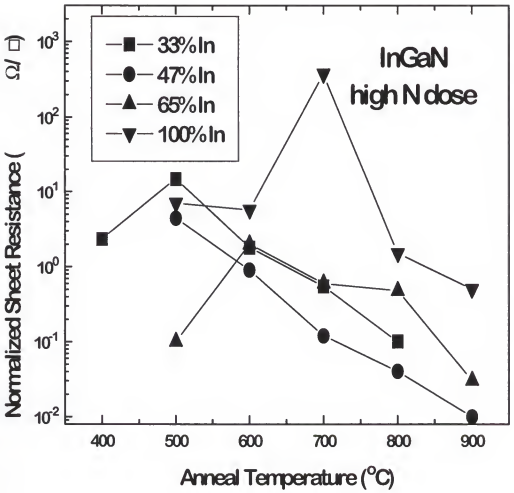

Figure 19. Normalized sheet resistance ratio versus anneal temperature for $In_xGa_{1-x}N$ implanted with high doses of N^+ at multiple energies.

Examples of the measurement temperature dependence of sheet resistance, corrected for the temperature dependence of mobility, are shown in Figure 20 for $In_{0.33}Ga_{0.67}N$ implanted with a high dose of N^+, and annealed at either 500 °C, or 800 °C. In the former case, an activation energy of 0.40 eV is obtained. This is relatively high in the bandgap of this material (~2.8 eV). As discussed earlier, implant isolation is most effective when the damage-related states are at midgap, as in the case in the $Al_xGa_{1-x}As$ and $In_xGa_{1-x}P$ materials systems.[20] The behavior of InAlN and InGaN is similar to that of InP and InGaAs,[20,22,24,26] where the damage-related levels are relatively high in the gap. The result is that initially n-type material achieves only moderate resistivities upon implantation with non-chemically active ions. The other side of this situation is that if one starts with initially p-type InP one can achieve very high resistivities because the Fermi level moves from near the valance band and through midgap on its way to the states in the upper part of the band and therefore an optimum choice of dose can place the Fermi level at midgap. To date no one has produced strongly p-type InGaN or InAlN, but it will be interesting to see if this behavior is observed in these materials. Upon annealing at 800 °C where it again becomes very conducting, the N^+ implanted $In_{0.33}Ga_{0.67}N$ displays an

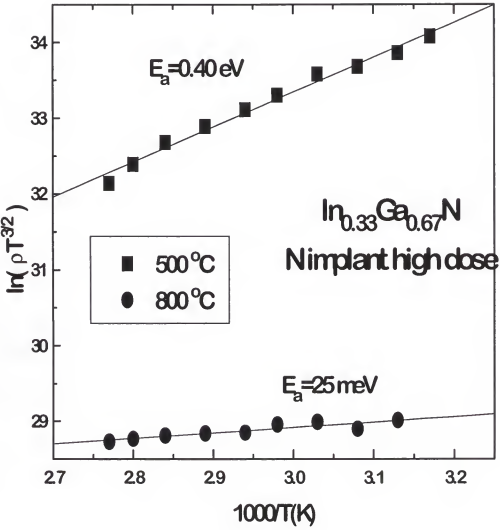

Figure 20. Arrhenius plots of sheet resistance of N^+ implanted $In_{0.33}Ga_{0.67}N$ implanted with a high dose of N^+ and subsequently annealed at either 500 °C or 800 °C.

activation energy of only ~25 meV, consistent with the values obtained in as-grown samples.

In summary, $In_xAl_{1-x}N$ and $In_xGa_{1-x}N$ samples were implanted with N^+ ions at various doses to understand their implant isolation characteristics. The sheet resistances were maximized by annealing at 600-700 °C, with increases up to 4 orders of magnitude for InAlN and generally an order of magnitude lower for InGaN. The conductivity under these conditions is controlled by implant-damage related deep acceptor states in the upper part of the bandgap. Annealing at higher temperatures restored the initial conductivity in both InAlN and InGaN. For electronic device isolation it appears that $In_xAl_{1-x}N$ can be made sufficiently resistive by implantation, whereas the initial conductivity of $In_xGa_{1-x}N$ will determine whether or not implantation will be successful for isolation. The demands for photonic devices are less restrictive and implantation should work well in gain-guided laser structures. Future work should concentrate on finding implant species that create chemically stable isolation, and on the behavior of p-type InAlN and InGaN.

Ion Implantation Doping Of GaN

The undoped GaN used in these experiments had n-type background carrier concentrations of $1\text{-}4x10^{16}$ cm^{-3}. These wafers were implanted with either $^{28}Si^+$ ($5x10^{14}$ cm^{-2}, 200

keV), $^{24}Mg^{+}$ ($5x10^{14}$ cm^{-2}, 180 keV) or $^{24}Mg^{+}/^{31}P^{+}$ ($5x10^{14}$ cm^{-2}, 180/250 keV) in an attempt to produce n- or p-type doping. Post implant annealing in the range 700-1100 °C for 10 sec was performed in a SiC coated graphite susceptor with the wafers in a face-to-face geometry. Electrical characterization was performed by Van der Pauw Hall measurements usig alloyed (350 °C, 10 sec) HgIn contacts at the corners of each sample.

Figure 21 shows the sheet resistance as a function of annealing temperature for Si^{+}, Mg^{+}, Mg^{+}/P^{+} and unimplanted GaN. There are several key features in the data:

(i) Mg^{+} implantation alone does not produce any noticeable doping effects under our conditions, and in fact the sheet resistance of these samples is slightly higher than the unimplanted control material, due presumably to the compensating lattice damage introduced.

(ii) annealing by itself above 1000 °C produces a slight increase in n-type conductivity in GaN, which may result from creation, or depassivation of the defects or impurities responsible for the as-grown doping (i.e., N-vacancy related defects or chemical impurities such O or Si[81]). The latter impurities may come from the susceptor or growth ambient, and can act as donors in GaN.

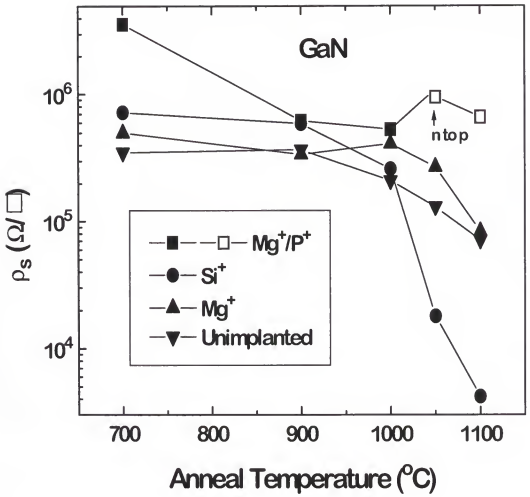

Figure 21. Sheet resistance of nominally undoped GaN either unimplanted, or implanted at a dose of $5x10^{14}$ cm^{-2} with Si^+ (200keV), Mg^+ (180 keV) or Mg^+/P^+ (180/250 keV) and subsequently annealed between 700-1100 °C.

(iii) Mg^+/P^+ co-implantation produces a sharp n-to-p conversion in conductivity after annealing at 1050-1100 °C, with creation of p-type material as determined by the sign of the Hall voltage and by thermal probe measurements. The sheet p-type doping obtained at 1100 °C is 9.46×10^{11} cm^{-2}, or an activation percentage of ~ 62%, since only 1.53×10^{12} cm^{-2} of the 5×10^{14} cm^{-2} implanted acceptors will be ionized assuming an energy level of 150 meV for Mg.[16] The effect of the co-implant is to increase the vacancy concentration and promote substitutionality of the Mg upon annealing.

(iv) Si^+ implantation produces a sharp increase in n-type conductivity upon annealing at 1050-1100 °C. The sheet electron density measured was 4.25×10^{13} cm^{-2}, or ~ 93% activation percentage assuming an energy level of 62 meV for Si.[1]

In conclusion, both donor and acceptor activation have been achieved in implanted GaN, using Si^+ and Mg^+/P^+, respectively. Annealing above 1050 °C was required to produce electrical activation of the implanted species. The activation percentages are in the range 62-93% when the ionization energy levels of the dopants is accounted for.

CHAPTER 4

MECHANISMS OF ETCHING

Wet Etching

Wet chemical etching of semiconductors has two basic steps, oxidation (or reduction) of the semiconductor surface, and removal of the soluble etch product. The slowest step in this process is therefore rate-limiting. In a diffusion limited etch, either the rate at which the active species diffuse to the surface of the semiconductor, or the diffusion of the soluble product away from the surface is the limiting process. This is not desirable from the view point of reproducibility, as the agitation of the solution is difficult to control, and this type of etch is extremely sensitive to agitation. For diffusion-controlled mixtures, etch rate is relatively insensitive to the temperature of the solution. The rate of etching may also be controlled by the speed of the chemical reaction at the semiconductor surface. This does not depend on agitation, but rather the temperature and pH of the solution. These factors are more easily controlled than solution agitation, and reaction-limited etches are preferred for device fabrication. One problem with III-V semiconductors is that

there are at least two different sublattices, each with its own reaction rate. Preferential etching may occur, which is not desired. It is possible to determine which is the rate limiting step from:

$$R = Ke^{Ea/kT}$$

Where R is the etch rate, K is a temperature dependent constant, E_a is the activation energy, T is the absolute temperature, and k is Boltzman's constant. Activation energies with values $\leq$ 6 kcal•mol^{-1} indicate diffusion-limited etching, while etches with values > 6 kcal•mol^{-1} are reaction-limited.

Wet etching has the advantage of being simple and inexpensive, does not damage the semiconductor surface and allows high throughput; because it tends to be isotropic, the undercutting of the masks makes it inapplicable for use with features less than 2 μm in size. This places an emphasis on the development of dry etch techniques for small geometry patterning.

Dry Etching

Dry etching proceeds by either physical sputtering, chemical reaction or some combination of the two. The purely chemical mechanism involves reactive gas molecules generated in the plasma chemically reacting with the

materials on the wafer surface. Volatile byproducts are created, which are pumped away. This is an isotropic etch.

The physical mechanism involves bombarding ions incident on the sample surface. Ions are accelerated toward the wafer surface through the use of an electrical bias, and with high enough energy, can physically remove material through a sputtering action. This etch mechanism is directional, making it possible to achieve highly anisotropic profiles. Many etches are a combination of physical and chemical mechanisms, with both reactive gases and energetic ions being present. While physical etches are anisotropic, (i.e. Ar^+ milling) they tend to be slow, have poor selectivity over mask materials and create significant lattice damage. Chemical etches tend to be faster, (usually based on chlorine, methane or fluorine gases) but are isotropic. An advantage of combining the mechanisms is that ion sputter-desorption of the reacted products can speed the etch. By selecting the right set of parameters, it is possible to get a fast etch that is also anisotropic, and has the desired selectivity. Residue needs to be minimized, as the contamination causes problems, as does plasma damage due to ion bombardment or nonuniformities in the plasma.

In order to produce small feature sizes, the process pressure in the etch reactor must be low. At lower pressure the mean free path of the molecules and ions are longer, and

there are fewer scattering-collision that reduce profile control. However, as the pressure decreases, the ease of which a plasma can be generated increases. Unless the disociation efficiency is increased, lowering the pressure lowers the density of ions and active neutrals. One solution is a high density plasma source, such as the electron cyclotron resonance (ECR) reactor.

In an ECR discharge, the plasma density is controlled separately from the ion energy. 2.45 GHz microwave energy is strongly absorbed in the plasma near the resonance magnetic field of ~ 875 G. Above that field, the waves propagate into the plasma, energizing electrons that create radicals, ions and active neutrals. Ions are accelerated to the substrate by a separate dc bias, with is independently controlled. Etching is done at the substrate by the ion and neutral flux produced in the plasma.

ECR sources have several advantages over conventianal parallel plate plasma etchers. ECR sources operate at lower pressure, (0.2-10 mTorr), compared to reactive ion etching (RIE), (50-100 mTorr). These sources create high density plasmas, (~ 10^{11}-10^{12} cm^{-3}), compared to typical RIE tools (~10^{9}-10^{10} cm^{-3}). Independent control of the plasma density and ion energies allows optimization of the etch. Reducing the physical nature of the etch can increase etch selectivity between materials, which is chemically

dependent. Physical damage to the substrate from high energy ion bombardment can also be reduced.

CHAPTER 5

WET CHEMICAL ETCHING

Introduction

There has been little success in developing wet etch solutions for the nitrides because of their chemical stability. High rates have been achieved in dry etch chemistries, but damage may be introduced by ion bombardment, and controlled undercutting is difficult to attain. In addition, since dry etching has a physical etch component, the selectivities between different materials is generally limited.

Amorphous AlN has been reported to etch in 100 °C HF/H_2O,[82-84] HF/HNO_3,[85] and NaOH,[86] and polycrystalline AlN in hot (≤ 85 °C) H_3PO_4 at rates less than 500 Å/min.[87,88] Mileham et al.[63] reported the etching of AlN defective single crystals in KOH based solutions at etch temperatures ranging from 23- 80 °C. They reported decreasing etch rates with increasing crystal quality, as the reactions occur favorably at grain boundaries and defect sites. InN in aqueous KOH solutions was reported to etch at a few hundred angstroms per minute at 60 °C.[89]

A compilation of wet etches tried for the III-nitrides is shown in Table II. Volume ratios were 1:1 for the mixtures. Lift-off indicates that there was a delamination of the epitaxial film from the GaAs substrate rather than etching of the nitride layer. This is due to the etch solution attacking the interface between the two materials that is defective and is usually a mixture of interdiffused material phases. There is a high density of stacking faults and dislocations in this region due to the lattice mismatch.[8] AZ400K, a KOH based solution, was found to etch AlN and InAlN. This solution was found to have no etch for $Al_xGa_{1-x}N$ (x=0.2 and 0.31).

As discussed previously, it has been reported that the luminescence and surface morphologies of GaN annealed in flowing N_2 actually improved for RTA temperatures up to 1100 °C. Thus one might expect that annealing of group III-nitrides would affect their wet etching characteristics. This is of critical importance as AlN is a good candidate as a capping material for other III-nitrides due to its thermal stability and the availability of a selective wet etch for removal. In the following section the effects of annealing on the wet etch rate of sputtered AlN films in KOH-based solutions is described, and also a study of the wet etch characteristics of $In_xAl_{1-x}N$.

Experimental

The AlN was reactively sputter deposited on a Si substrate to a thickness of ~ 1200 Å using a N_2 discharge and a pure Al target. This type of AlN film has been shown to be an effective annealing cap for GaN at a temperature of 1100 °C.[90] The $In_xAl_{1-x}N$ films were either conducting n-type as-grown (~ 10^{18} cm^{-3}) for $x \geq 0.03$due to residual autodoping by native defects or fully depleted for $x < 0.03$, and were grown on GaAs or Si substrates. The material grown on GaAs was of superior quality. Not only is GaAs a polar substrate, but it was exposed to a nitrogen plasma prior to growth, and formed a thin GaN layer which served as a template for subsequent growth. The compositions examined were 100, 75, 36, 29, 19, 3.1, 2.6 and 0 % In.

The AlN samples were annealed in a rapid thermal anneal (RTA) system (AG 410T) face down on a GaAs substrate for 10 s at temperatures between 500 - 1150 °C in a N_2 atmosphere. For wet etching studies, all samples were masked with Apiezon wax patterns. Etch depths were obtained by Dektak stylus profilometry after the removal of the mask, with an approximate 5% error. SEM was used to examine the undercutting on the etched samples. AZ400K developer solution, with an active ingredient of KOH,[63] was used for the etch, at temperatures between 20 and 80 °C.

Table II. Compilation of etching results in acid and base solutions, performed at room temperature (25°C) unless otherwise noted.

	GaN	InN	AlN	InAlN	InGaN
Citric Acid (75 °C)	0	0	0	0	0
Succinic Acid (75 °C)	0	0	0	0	0
Oxalic Acid (75 °C)	0	lifts off	lifts off	lifts off	lifts off
Nitric Acid (75 °C)	0	lifts off	0	lifts off	lifts off
Phosphoric Acid (75 °C)	0	0	0	0	0
Hydrochloric Acid (75 °C)	0	0	0	0	0
Hydrofloric Acid	0	lifts off	0	0	lifts off
Hydroiodic Acid	0	0	0	0	0
Sulfuric Acid (75 °C)	0	lifts off	0	0	0
Hydrogen Peroxide	0	0	0	0	0
Potassium Iodide	0	0	0	0	0
2% Bromine-Methanol	0	0	0	0	0
n-Methyl-2-Pyrrolidone	0	0	0	0	0
Sodium Hydroxide	0	lifts off	lifts off	lifts off	lifts off
Potassium Hydroxide	0	lifts off	22650 Å/min[5]	lifts off	0
AZ400K photoresist developer (75 °C)	0	lifts off	~60-10000 Å/min	0-16000 Al fn of x	0
Hydroiodic Acid/hydrogen peroxide	0	0	0	0	0

Hydrochloric Acid/hydrogen peroxide	0	0	0	0	0
Potassium Triphosphate (75 °C)	0	0	0	0	0
Nitric Acid/ Potassium Triphosphate (75 °C)	0	lifts off	0	0	0
Hydrochloric Acid/Potassium Triphosphate (75 °C)	0	0	0	0	0
Boric Acid (75 °C)	0	0	0	0	0
Nitric/Boric Acid (75 °C)	0	lifts off`	0	0	lifts off
Nitric/Boric/Hydrogen Peroxide	0	lifts off	0	0	removes oxide
$HCl/H_2O_2/HNO_3$	0	lifts off	0	lifts off	lifts off
Potassium Tetraborate (75 °C)	0	oxide removal	oxide removal	oxide removal	oxide removal
Sodium Tetraborate (75 °C)	0	0	0	0	0
Sodium Tetraborate/Hydrogen Peroxide	0	0	0	0	0
Potassium Triphosphate (75 °C)	0	0	0	0	0
Potassium Triphosphate /Hydrogen Peroxide	0	0	0	0	0

Results And Discussion

(a) AlN

Figure 22 shows the etch rate of the sputtered AlN as a function of etch temperature for samples as-deposited or annealed at 500, 700, 900, 1000 and 1100 °C. The etch rates of both the as-deposited and 500 °C annealed sample increase sharply as the etch temperature increases from 20 to 50 °C, and then level off; the rate drops by approximately 10 % with a 500 °C anneal. The samples annealed at 700, 900 and 1000 °C also show similar trends, with a monotonic decrease in rate for higher anneal temperatures. The crystal quality appears to increase significantly with anneal temperature, as the etch rate drops accordingly. The etch rate continues to drop by ~ 10 % with each successive 100 °C increase in anneal temperature, up to 1000 °C. After the 1100 °C the etch rate drops and is less temperature dependent. Overall there is an ~ 90 % reduction in etch rate from the as-deposited AlN to that annealed at 1100 °C for etching at 80 °C.

The activation energy for an etch solution can be determined from an Arrhenius plot, and is shown in Fig. 23. The activation energies for all samples was the same within

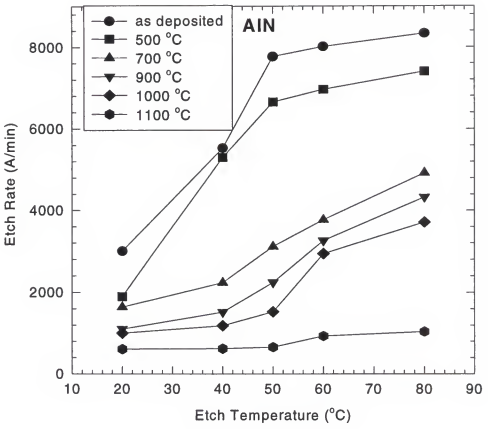

Figure 22. Etch rate of AlN as a function of etch temperature for samples as-deposited or annealed at 500, 700, 900, 1000 and 1100 °C.

experimental error, 2.0 ± 0.5 kcal•mol^{-1}, which is indicative of a diffusion limited reaction. This is much lower than the activation energy of 15.45 kcal•mol^{-1} reported by Mileham et al,[15] for AlN grown by metal organic molecular beam epitaxy. The quality of the material in the current experiment is much lower though, and the etch may be proceeding at such a rapid rate that the solution is becoming depleted of reactants near the materials surface. The fact that the activation energy is the same for all quality material indicates that the etch proceeds by the same mechanism in all grades material. The number of broken or defective bonds is higher in poorer quality AlN, thus the number of attempt frequencies is greater, and the etch faster.

(b) $In_xAl_{1-x}N$

The etch rate as a function of solution temperature for $In_xAl_{1-x}N$ grown on either GaAs or Si, for 19 % In is shown in Fig. 24. At 20 °C etch temperature there is no difference in etch rate. The etch rates for both materials increase with etch temperature, with the differential in etch rates also increasing with temperature. As was mentioned previously, the InAlN grown on Si has a greater concentration of crystalline defects as evident from x-ray diffraction and absorption measurements. At 80 °C the etch

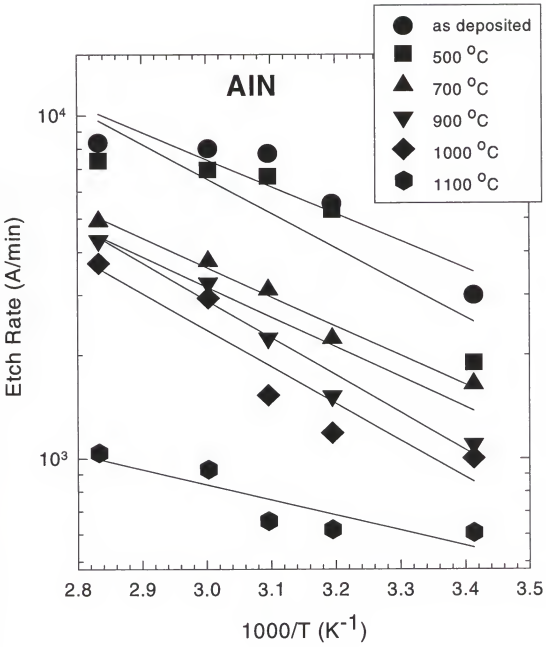

Figure 23. Arrhenius plots of etch rates for as-deposited or annealed AlN as a function of reciprocal etch temperature.

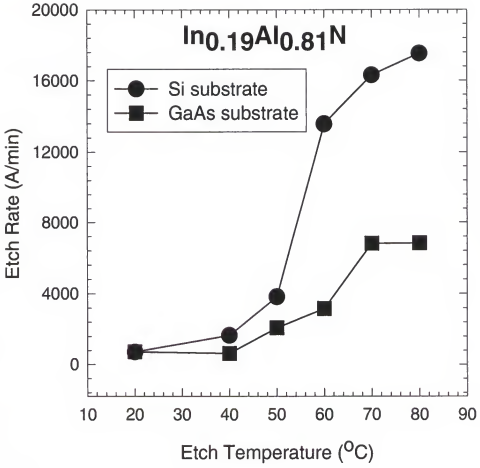

Figure 24. Etch rates as a function of etch temperature for $In_xAl_{1-x}N$ grown on GaAs and Si, for 19% In.

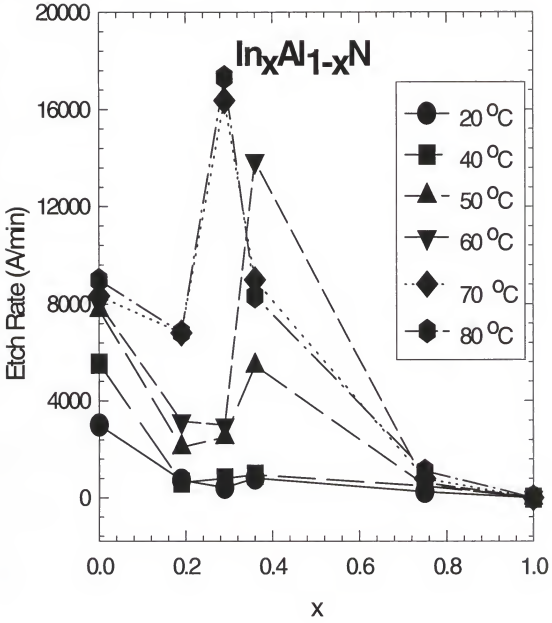

Figure 25. Etch rate for $In_xAl_{1-x}N$ for $0 \leq x \leq 1$ grown on GaAs at solution temperatures between 20 and 80 °C.

rate for the film on the Si substrate is approximately three times faster than for the film grown on GaAs. This is another clear indication of the dependence of wet etch rate on material quality, and emphasizes why it has proven very difficult to find etch solutions for high quality single-crystal nitrides.

Etch rates for $In_xAl_{1-x}N$ grown on GaAs for $0 \leq x \leq 1$ are shown in Fig. 25, for etch temperatures between 20 and 80 °C. Up to 40 °C, the etch rates are very low and show little dependence on In composition. The AlN etches much faster at these temperatures than any composition of the ternary alloy InAlN. As the etch temperature increases to 60 °C, the etch rates increase, showing a peak for 36% In. This is presumably due to tradeoff between the reduction in average bond strength for InAlN relative to the pure binary AlN, and the fact that the chemical sensitivity falls off at higher In concentrations. Thus the etch rates initially increase for increasing In, but then decrease at higher concentrations because there is no chemical driving force for etching to occur. InN did not etch in this solution at any temperature, but was occasionally lifted off during long etches because of the defective interfacial region between InN and GaAs being attacked by the KOH.

Arrhenius plots of etch rates for $In_xAl_{1-x}N$ for $0 \leq x \leq 1$ with associated activation energies for the etches are

shown in Fig. 26. There is substantial scatter in the data, but the activation energies are all in the range 2-6 $kcal \bullet mol^{-1}$, which again is consistent with diffusion-controlled etching. This is not desirable for device fabrication processes because the rates are then dependent on solution agitation and the etched surface morphology are generally rougher than for reaction-controlled solutions.

Apart from material quality or composition, another factor which often plays a role in determining etch rates is sample conductivity. Figure 27 shows a plot of InAlN etch versus etch rate temperature for samples with 2.6% and 3.1 % In, which were depleted ($n < 10^{16}$ cm^{-3})and doped at $n \sim 5x10^{18}$ cm^{-3}, respectively. Since the autodoping changes rapidly around this composition, but there is little change in In concentration, these samples represent a good test of any effects related to conductivity. The samples have similar etch rates at low solution temperatures. Above 60 °C, however, the n-type sample etch rate increases more rapidly, approximately two times faster than the depleted sample. These results indicate that at temperatures where fast etch rates occur, the electrons in the n-type sample are part of the chemical reaction between the OH^- ions and the Al in the InAlN film. They may enhance formation of

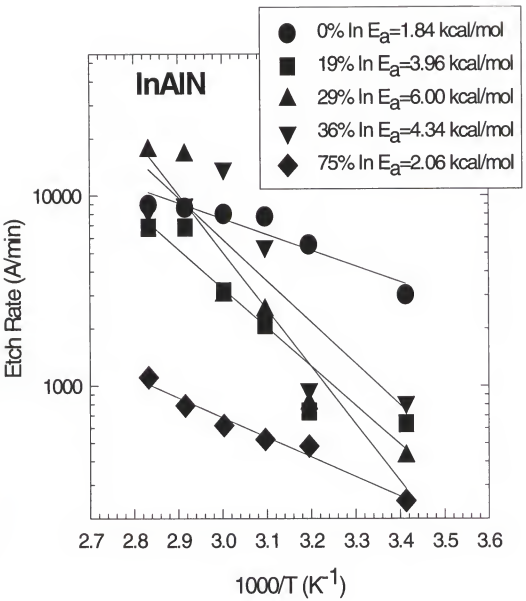

Figure 26. Arrhenius plots of etch rates for $In_xAl_{1-x}N$ for $0 \leq x \leq 1$ as function of reciprocal etch temperature, giving activation energy for etch.

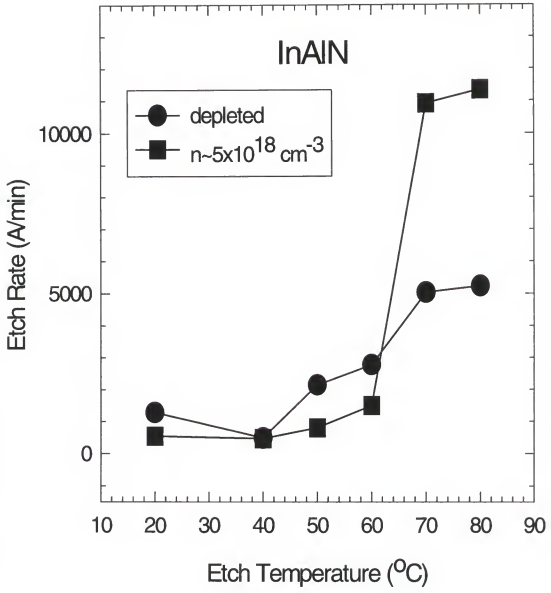

Figure 27. Etch rate for n-type (3.1% In) and depleted InAlN (2.6% In) as a function of solution temperature.

these ions initially and thus the etch rate is increased. It will be interesting to examine results for p-type InAlN, where the electrons are absent.

Etching with KOH-based solution is completely selective for InAlN over GaN or InN. As an example Fig. 28 shows an SEM micrographs of the feature etched into a GaN/InGaN/AlN heterostructure that was first patterned by Cl_2/Ar ECR dry etching (top) and then wet etched for 5 mins at 60 °C in the AZ400K solution (middle and bottom). Only the AlN is etched under these conditions.

Conclusions And Summary

Annealing of sputtered AlN improved the crystal quality of the film, decreasing the chemical etch rate in KOH-based solutions. InAlN etch rates also increased with decreasing crystalline quality. Both AlN and InAlN samples had activation energies for etching in KOH $\leq$ 6 kcal$\bullet$mol^{-1}, which are typical of a diffusion-controlled etch mechanism. The etch rate for the InAlN initially increased as the In composition increased from 0 to 36%, and then decreased to zero for pure InN. The n-type InAlN etched approximately two times faster than the undoped material above 60 °C, indicating that electrons play a role in the etch mechanism.

Figure 28. SEM micrograph of selectively undercut GaN/InGaN/AlN heterostructure, showing the high selectivity for the AZ400K solution to etch only Al-containing nitrides. The feature was first patterned by Cl_2/Ar ECR dry etching (top) and then wet etched for 5 mins at 60 °C in the AZ400K solution (middle and bottom). The scale is 1 inch equals 0.5 μm in the center micrograph.

CHAPTER 6

DRY ETCHING

Electron Cyclotron Resonance Etching Versus Reactive Ion Etching

It has proven difficult to develop wet etching solutions for the nitrides based on conventional acids and bases, and attention has been focused on dry etching techniques. One would expect that high ion density etching methods such as Electron Cyclotron Resonance (ECR) would be advantageous for the nitrides for two reasons:

(i) more efficient sputter-enhanced removal of etch products, which is strongly dependent on ion energy, and more efficient initial bond breaking so that the etch products may actually form.

(ii) higher concentration of reactive species which enhances the chemical component of the etch mechanism.

A compilation of the boiling points of the possible etch products is in Table III. It is expected that group III chloride or metalorganic group III compounds, and various N compounds will be the etch

Table III: Boiling Points of III-V Etch Products*

Species	Boiling Point (°C)	Species	Boiling Point (°C)
$GaCl_3$	201	NCl_3	< 71
$GaBr_3$	279	NI_3	explodes
GaI_3	sub 345	NF_3	-129
$(CH_3)Ga$	55.7	NH_3	-33
		N_2	-196
$InCl_3$	600	$(CH_3)_3N$	2.9
$InBr_3$	> 600		
InI_3	210	PCl_3	76
$(CH_3)_3In$	134	PBr_5	106
		PH_3	-88
$AlCl_3$	183		
$AlBr_3$	263	$AsCl_3$	130
AlI_3	191	$AsBr_3$	221
$(CH_3)_3Al$	126	AsH_3	-55
		AsF_3	-63

*CRC Handbook of Chemistry and Physics (CRC Press, Boca Raton, FL 1990).

products, depending on the exact plasma chemistry employed. From the data in Table III one would expect to be able to rapidly etch GaN and related alloys in Cl_2 chemistries (with ion assistance for In containing alloys), I_2 chemistries, Br_2 chemistries (with ion assistance again to remove $InBr_3$) or CH_4/H_2, i.e. the normal plasma mixtures used for conventional III-V's such as GaAs. However under typical reactive ion etch conditions the etch rates reported for the nitrides are factors of 5-10 lower than for conventional III-V semiconductors under the same conditions. While GaN comprises the cladding layer in InGaN quantum well lasers and LED's, it is also important to investigate related materials because they are important for the development of more advanced nitride based devices. It should be noted that Table III is an oversimplification, since other factors such as polymer deposition, selvedge layer formation, bond strengths and other factors affect etch rates under plasma conditions.

A number of investigations of dry etching of GaN in various chemistries have been done in both reactive ion etching, (RIE),[91-94] and electron cyclotron resonance (ECR) modes.[95-98] AlN and InN ECR etching has also been reported.[98] Shul et al have compared etch rates for the RIE versus ECR

etching of GaN in a $Cl_2/CH_4/H_2/Ar$ plasma and found much lower rates for the RIE conditions.[9]

A comparison of RIE and ECR etching of GaN, AlN, InN and InGaN was made in Cl_2/Ar and $CH_4/H_2/Ar$ plasmas using the same reactor, plasma chemistries and etch conditions. The GaN and AlN were resistive as-grown, the InN was highly autodoped n-type ($>10^{20}$ cm^{-3}) due presumably to the presence of native defects, and the InGaN was also n-type ($\sim10^{19}$ cm^{-3}). The samples were patterned with a carbon-based mask, and were etched in a Plasma-Therm SLR 770 reactor with an Astex 4400 low profile ECR source. The ECR cavity was formed with an upper magnet (170 A) and collimated with an lower magnet (40 A). The process pressure was held constant at 1.5 mTorr and the temperature of the rf powered, He back-side cooled chuck was held at 23 °C. The rf power (13.56 MHz) varied between 0 and 450 W and the microwave power was held at either 0 or 1000 W for RIE and ECR conditions respectively. The plasma chemistries used were 5 sccm Cl_2 / 10 sccm Ar or 5 sccm CH_4 / 15 sccm H_2 / 10 sccm Ar. Step heights were obtained from Dektak stylus profilometry measurements after the removal of the mask with acetone, and used to calculate the etch rates. The error in these measurements is approximately ~ 5 %. The surface morphology of the etched InN samples was examined with an AFM using a Si tip in tapping mode. The InN was expected to be the most

susceptible to morphology changes because of its lower bond strength and difference in mass between the lattice constituents. Therefore it serves as a worst case scenario for the other nitrides in terms of sensitivity to the effects of changing plasma parameters.

Results And Discussion

Figure 29 shows a plot of the etch rate of AlN and GaN in $CH_4/H_2/Ar$ discharges as a function of rf power for RIE and ECR conditions. Under RIE conditions, the GaN etch rate increased with rf power to 250 W and thereafter showed little change. The rf-induced dc bias increases from -20 V to -275 V under these conditions. The average ion energy is the sum of this accelerating voltage, plus the plasma potential (~30V). The GaN etching was etch product formation or reactant-limited under these conditions, as evidenced by the increase in rate with increased ion energy. The rates for ECR etched GaN increased sharply with rf power to 150 W and then increased more gradually thereafter as the ion energy was sufficiently high to efficiently desorb all the etch products formed at this particular pressure and flow rate. Under ECR conditions, the dc self-biases ranged from -10 V to -160 V; these values are lower than for the RIE case because the higher ion density suppresses the cathode dc bias. Microwave interferometry measurements in our reactor

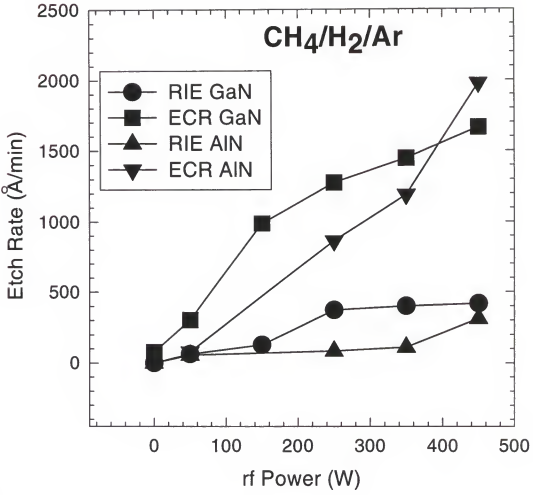

Figure 29. AlN and GaN etch rates as a function of rf power for RIE and ECR generated $CH_4/H_2/Ar$ plasmas (1.5 mTorr).

show typical ion densities of ~ $3x10^{11}$ cm^{-3} for $CH_4/H_2/Ar$ at 1000 W microwave power (ECR conditions), and ~ $2x10^{9}$ cm^{-3} at 0 W (RIE conditions). Optical emission intensities of standard Ar lines and the 656.2 nm atomic hydrogen line are also typically an order of magnitude higher under ECR conditions. The ECR mode provided a higher density of species needed for formation of the Ga etch products, and a higher ion density for the sputter removal of these products; in RIE mode the degree of sputtering was simply not high enough to get efficient removal of material. The role of high ion flux under ECR conditions is two-fold. First it increases the initial bond-breaking, allowing the etch products to form, and second, it produces efficient sputter-assisted desorption of these products.[6-9] The concentration of reactive species and ions was less in the RIE mode, and the etch rate slower. Table IV shows that there is a reasonable correlation between etch rate and material bond energy[100] and no correlation to product volatility,[101] demonstrating that the high ion density in the ECR plasma enables product formation and desorption even when the products have low volatility. The etch rates of the nitrides actually fall with increasing pressure at fixed rf power, indicating that bond-breaking and not limited reactants is the rate limiting step. The AlN etch rate increased linearly with rf power in both RIE and ECR modes,

Table IV. Bond strengths of III-Nitride semiconductors (GaAs shown for reference).[10]

Material	Bond Strength (eV/atom)	Etch Rate(Å/min) $CH_4/H_2/Ar$ 250W rf, 1000 W ECR
AlN	11.52	~800
GaN	8.63	~1300
InN	7.72	~2100
GaAs	6.52	~2250

though much more sharply in the ECR. At 450 W, however, the etch rates for RIE and ECR increased sharply indicating enhanced sputter desorption by the ions. The GaN etch rates were approximately four times faster in the ECR than in the RIE, independent of rf power, whereas the AlN etch rate in the ECR was four times faster above 50 W. At 450 W the sputtering ions may have enough energy to break the AlN bonds directly, thus increasing the etch rate for this material. It is expected from past results on $CH_4/H_2/Ar$

etching of other III-V's that GaN will have slower rates than In-containing materials.[102]

Figure 30 shows the $CH_4/H_2/Ar$ etch rates for InN and InGaN as a function of rf power for RIE and ECR conditions. The RIE etch rate for both these materials is very low and independent of rf power indicating that the etch products are inefficiently formed under these conditions. The ECR etch rate for InN was high in this chemistry for all rf powers, and increased with increasing rf power due to more efficient sputter desorption. The InGaN follows a pattern that could be expected from the combination of the etch rates of the two components, GaN and InN. The ECR etch rates for InN and InGaN are faster by approximately a factor of ten than the RIE etch rates. The Cl_2/Ar etch rates of AlN and GaN as a function of rf power for RIE and ECR conditions are shown in Fig. 31. GaN was etched much faster than AlN in the chlorine chemistry in either mode. This is again consistent with the higher bond strengths of AlN, so that the etch products are initially more difficult to form for this material. Above 50 W the etch rates for both materials under RIE and ECR conditions increase monotonically with rf power. The GaN ECR etch rate was approximately a factor of four times higher than the RIE etch rate, and the AlN ECR rate was about an order of magnitude faster than the RIE

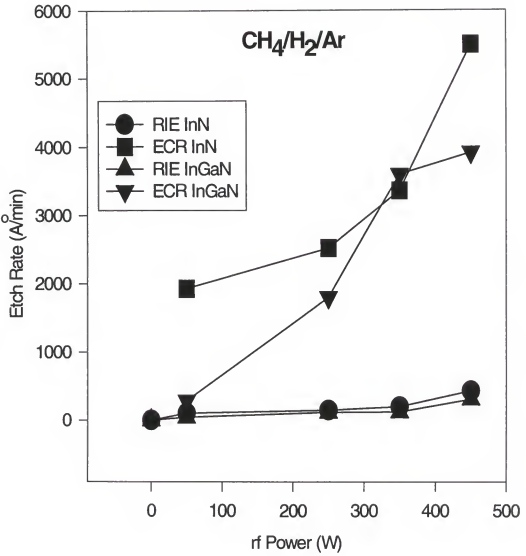

Figure 30. InN and InGaN etch rates as a function of rf power for RIE and ECR generated $CH_4/H_2/Ar$ plasmas (1.5 mTorr).

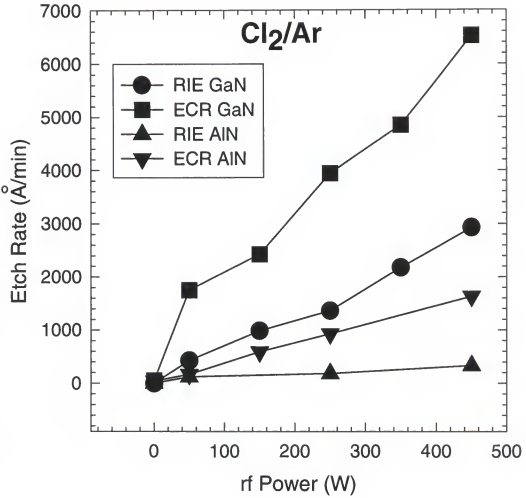

Figure 31. AlN and GaN etch rates as a function of rf power for RIE and ECR generated Cl_2/Ar plasmas (1.5 mTorr).

rate. The GaN was etched much faster in the chlorine chemistry than the methane based discharges (approximately five times faster in RIE, and three times faster in ECR). This is not expected from Table III, where the volatility of the metalorganic Ga species is higher than that of $GaCl_3$, but as described earlier other factors such as film deposition or formation on the plasma-exposed surface may dominate the final etch rate. The AlN was etched slightly faster in the methane chemistry than the chlorinechemistry in ECR mode, and the etch rates were basically the same in both chemistries in RIE mode. This is expected from the data of Table III since the metalorganic Al species are more volatile than the $AlCl_3$.

Figure 32 shows the Cl_2/Ar etch rate of InN and InGaN as a function of rf power for both RIE and ECR conditions. In RIE mode, the etch rate was again very low for both materials. In ECR mode the etch rate increased rapidly as the rf increased from 0 to 50 W, indicating that there is a threshold ion energy for forming and removing the by-products. Above 50W, the etch rates increased slowly until 150 W for InN and 250 W for InGaN, at which point the etch rates increased more rapidly. In the RIE mode for this chemistry, the GaN etched much faster than the InN. This is expected since $InCl_3$ is much less volatile than $GaCl_3$. InGaN

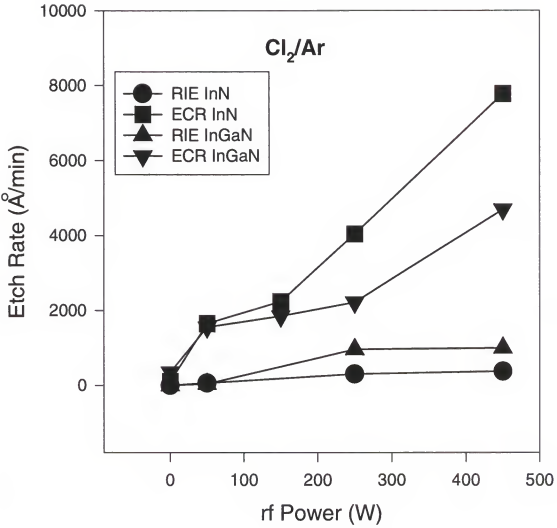

Figure 32. InN and InGaN etch rates as a function of rf power for RIE and ECR generated Cl_2/Ar plasmas (1.5 mTorr).

followed a trend similar to that of GaN. Both InN and InGaN etched faster in the chloride chemistry than in the methane chemistry for both modes. Thus the chloride etch products are more volatile than their metalorganic counterparts under ion-assisted conditions, although their equilibrium vapor pressures are generally lower. No polymer deposition was found on any of the $CH_4/H_2/Ar$ etched samples and exclude this as a possibility. However surface coverage of $(CH)_x$ species may impede etch product formation in some cases.

Figure 33 shows the root mean square (RMS) roughness versus rf power for the InN samples etched in $CH_4/H_2/Ar$ and Cl_2/Ar under ECR conditions. The $CH_4/H_2/Ar$ etched surface was actually smoother than the as-grown sample surface for low powers, indicating that surface features are removed predominantly by sputtering. The surface got increasingly rougher as the rf power was increased, returning to the initial roughness at 250 W and increasing to a maximum of 70 nm at 450 W. Sharp features will be removed by ion milling faster than flat features because of the angular dependence of milling rate, and as long as preferential sputtering of N does not occur, this will lead to a degree of smoothing of the surface.[103] Once the ion energy is high enough to cause faster removal of the lighter N atoms the surface will roughen and become rich in the group III element, a fact confirmed by Auger Electron Spectroscopy analysis. The

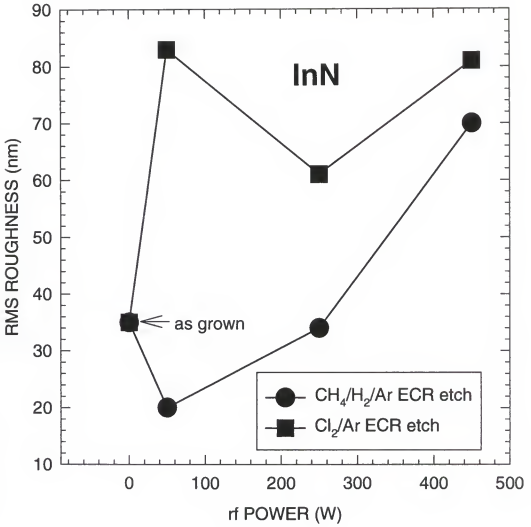

Figure 33. RMS roughness for InN samples etched in $CH_4/H_2/Ar$ and Cl_2/Ar discharges as a function of rf power under ECR conditions.

Cl_2/Ar etched surface was consistently rougher than the CH_4/H_2/Ar etched surface, but it should be added that these samples were etched much deeper. This is consistent with results on the Cl_2-based ECR etching of InP, where the low volatility of the In-chlorides results in preferential loss of the group-V species at room temperature,[12] leaving a rough surface. CH_4/H_2 plasmas at moderate ion energies, on the other hand, give slow, smooth etching of InP.[104] At higher ion energies, preferential loss of the P occurs, producing severe surface roughening. When the RMS roughness of the nitride samples was normalized to the etch depth the CH_4/H_2/Ar etched surface was rougher than the Cl_2/ Ar etched surface at 450 W. The roughness on the Cl_2/Ar etched samples decreased ~ 25 % from 50 W (rms = 83 nm) to 250 W (rms = 60 nm) indicating that there is more efficient removal of In, and then increased again to 80 nm at 450 W, as preferential sputtering again predominates. The normalized RMS roughness followed a similar trend. The raw AFM scans of InN samples etched in CH_4/H_2/Ar and Cl_2/Ar under ECR conditions are shown in Fig. 34, illustrating the effects described above.

Summary

The etch rates of GaN, AlN, InN and InGaN were found to be significantly faster in ECR than in RIE conditions using

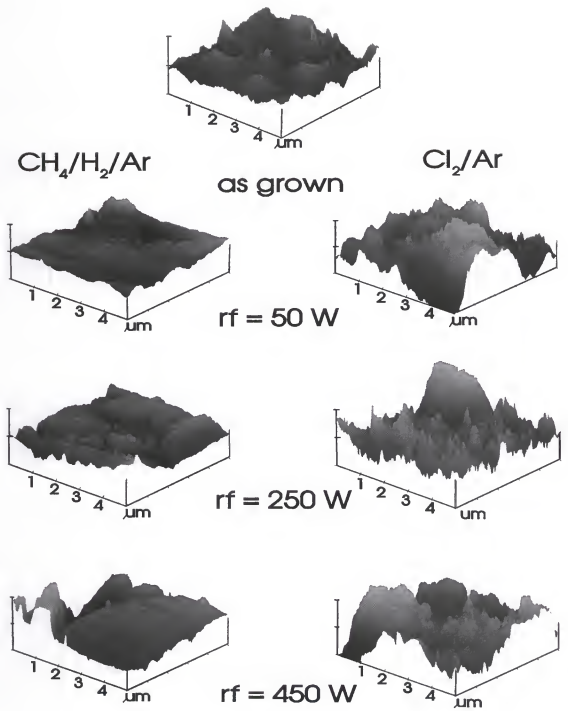

Figure 34. AFM scans of InN samples etched in $CH_4/H_2/Ar$ and Cl_2/Ar discharges as a function of rf powers under ECR conditions.

the same reactor and plasma conditions in Cl_2/Ar or $CH_4/H_2/Ar$ plasmas. This was due to the higher density of ions that can both break the nitride bonds allowing the etch products to form, and then efficiently desorb these products under ECR conditions. The Cl_2/Ar plasma chemistry was found to etch GaN, InN and InGaN faster than $CH_4/H_2/Ar$ due to the efficient desorption of the Cl-group III etch products under ion-enhanced conditions, while AlN was etched slightly faster in $CH_4/H_2/Ar$ plasmas in ECR mode. The GaN etch rate was higher than the InN in the Cl_2/Ar chemistry, and the InN was faster in the $CH_4/H_2/Ar$ plasmas as is typical for other III-V materials like GaAs and InP. The surface morphology of InN was the most sensitive to changes in plasma conditions and was found to be a strong function of both rf power and the etch chemistry under ECR conditions.

Etching Of III-Nitrides In ICl/Ar And IBr/Ar Plasmas

Introduction

Various new plasma chemistries have been explored in the search for a fast, smooth, anisotropic etch of the nitride materials. Surface roughness is often caused by preferential loss of the group V element from the surface due to its higher volatility. Iodine based etch products have a higher volatility for In and Ga than Cl_2 or CH_4 etch

products which could alleviate that problem and also result in faster etching (see Table III). The conventional etches are often rate limited by removal of the group III etch product. I-based etching of GaAs and $Al_xGa_{1-x}As$ has been investigated for in situ etching in OMVPE using CH_3I,[105,106] and for RIE etching of InP, InGaAs and InGaAsP with I_2/Ar and $HI/H_2/CH_4$ chemistries.[107] Smooth surfaces and relatively fast etch rate (~2000 Å/min) were achieved at optimum conditions. InP etching in RIE was also studied in CH_3I, CF_3I and CH_3I/O_2,[108] but there were problems with rough slow etches and polymer deposition. More recently Pearton et al. investigated the ECR etch of InP in $HI/H_2/Ar$[109] and found etch rates > 1 μm/min, smooth anisotropic etching with no residue after etch. This chemistry was also used to etch GaAs, InAs, InSb, InP, and GaSb,[110] reporting etches that were anisotropic, smooth, with no deposition during etch, and an order of magnitude faster than $CH_4/H_2/Ar$ etches. Less work has been done with Br_2-based plasma discharges. GaN has been etched in HBr, HBr/Ar, and HBr/H_2 under reactive ion etch conditions, with etch rates around > 600 Å/min at 400 V dc.[107] Somewhat faster rates were achieved under ECR conditions in HBr/H_2[111] (~900 Å/min at -150 V dc). Plasma chemistries based on ICl and IBr are of interest as plasma dissociation produces active chlorine or bromine and iodine and should provide efficient etching of the nitrides.

Experimental

The etch characteristics of GaN, AlN, InN, $In_{0.36}Al_{0.64}N$ and $In_{0.5}Ga_{0.5}N$ were investigated. The GaN and AlN were resistive as-grown, and the InN was highly autodoped n-type ($>10^{20}$ cm^{-3}), while the $In_{0.36}Al_{0.64}N$ and $In_{0.5}Ga_{0.5}N$ compositions employed were conducting n-type as-grown (~ 10^{19} cm^{-3}). The samples were patterned with either a carbon-based mask or photoresist, and were etched in a Plasma-Therm SLR 770 reactor with an Astex 4400 low profile ECR source. The ICl and IBr are crystalline solids with melting temperatures of ~ 23 and 50 °C respectively.[100] ~ 50 g of ICl or IBr were loaded into a stainless steel vacuum vessel directly connected to a mass flow controller which injected the vapor into the ECR source. The vacuum vessel was wrapped in Al-foil and heated to ~ 45 °C. An optical emission spectrum for a 1000 W ECR IBr discharge is shown in Fig. 35- there are many atomic I and Br lines, indicating efficient dissociation of this weakly bound molecule. Flow rates up to 12 standard cubic centimeters per minute (sccm) were obtained. The process pressure was held constant at 1.5 mTorr and the temperature of the He back-side cooled chuck was held at 23 °C. The rf power (13.56 MHz) was varied between 50 and 250 W and the microwave power between 400 and

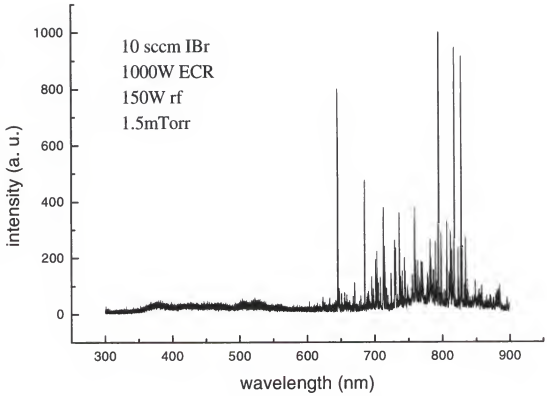

Figure 35. Optical emission spectrum of 1000 W ECR IBr discharge.

1000 W. The plasma chemistries used were ICl/Ar or IBr/Ar with respective flows of 4 sccm/4 sccm, 2 sccm/ 6 sccm, 1sccm/ 7 sccm and 8 sccm/ 0 sccm. Step heights were obtained from Dektak stylus profilometry measurements after the removal of the carbon mask with acetone, and used to calculate the etch rates, with an error in the measurements of approximately ~ 5 %. The surface morphology of selected GaN samples were examined with AFM using a Si tip in tapping mode and SEM, while near-surface composition was measured by AES.

Results And Discussion

The etch rates as a function of plasma composition for GaN, InN, InAlN, AlN and InGaN are shown in Fig. 36. Microwave power was held at 1000 W and rf power at 150 W (corresponding to a dc self bias of -170 V at the sample position). For the ICl based etch (Fig. 36, top), the GaN and InGaN etch rates rise as the amount of ICl in the etch increases from 12.5 to 50%, and then level off. Above 50% ICl there appears to be a competition between the formation of $GaCl_3$ with has a boiling point of 201 °C, with that of GaI_3 which sublimes at 345[112]. The $GaCl_3$ may form preferentially at some plasma compositions. The InN shows a sharp increase in etch rate above 25 % ICl. This suggests that at 25 % ICl the InI_3, which is much more volatile

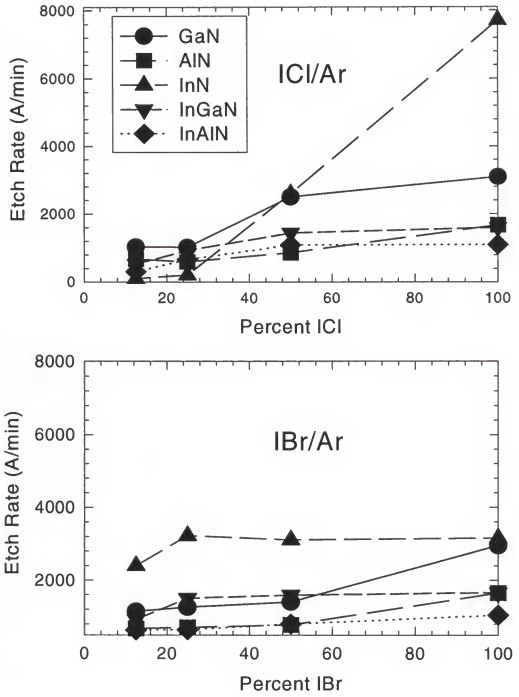

Figure 36. Etch rate as a function of percent ICl (top) or IBr (bottom) for GaN, InN, InAlN, AlN and InGaN in 1000 W (ECR), 150 W rf, 1.5 mTorr discharges.

($InCl_3$ boils at 600 °C, InI_3 at 210 °C), can form easily. The InAlN and AlN are not greatly effected by changes in the composition of the plasma in ICl (or IBr, Fig. 36, bottom), perhaps because both Al containing etch products have similar volatility ($AlCl_3$ boils at 183 °C, $AlBr_3$ at 263 °C and AlI_3 at 191 °C) and because the etch rate is probably limited by the initial bond breaking in the Al-containing materials. It is expect that AlN and InAlN will be difficult to etch because of their high average bond energies. The N containing etch products are much more volatile than the group-III etch products, with NCl_3 boiling at < 71 °C while NI_3 is explosive.

The etch rates for InN and InGaN increased as the amount of IBr in the etch increased from 12.5 to 25%, and remained constant at higher percentages (Fig. 36, bottom). This suggests that above 25 % IBr the etching is no longer reaction-limited. The $InBr_3$ etch product is much less volatile than InI_3, as mentioned earlier. Above that composition however, there may have been competition between the formation of $InBr_3$ and InI_3, which slowed the etch, or the etch may have been limited by the removal of the reactants from the surface. GaN etch rates showed little change with IBr composition to 50 % IBr plasma composition, but at 100 % IBr the etch rates increased sharply. There may not have been enough reactants at the etch surface at 50 %

IBr, or at these lower percents of IBr there may be a competition between the formation of $GaBr_3$ and GaI_3.

In Figure 37 the etch rate as a function of microwave power for GaN, InN, InAlN, AlN and InGaN is shown for values between 400 and 1000 W for ICl/Ar plasmas (top) and IBr/Ar (bottom). The rf power was etch rate dropped sharply at 800 W and then remains held at 150 W, and 4 sccm ICl or IBr / 4 sccm Ar gas flows were used. Both InAlN and AlN have low etch rates in ICl/Ar, and show no significant change in etch rate with increasing microwave power. This indicates that they are not reaction limited in this chemistry, since increasing the microwave power results in a higher concentration of reactive species which enhances the chemical component of the etch mechanism. GaN and InGaN showed a slight increase in etch rate from 400 W microwave power to 600 W. Thereafter the GaN etch rate dropped gradually with increasing microwave power, while the InGaN constant at 1000 W. This would indicate either a diffusion-limited etch, where the number of reactants becoming available exceeds the rate at which the iodine and/or chlorine etch products can be removed, or competition between reactants occurs above 600 W microwave power. The InN had a maximum in etch rate at 800 W ECR power. This might result from the large difference in volatilities of the etch products for this material, leading to a strong

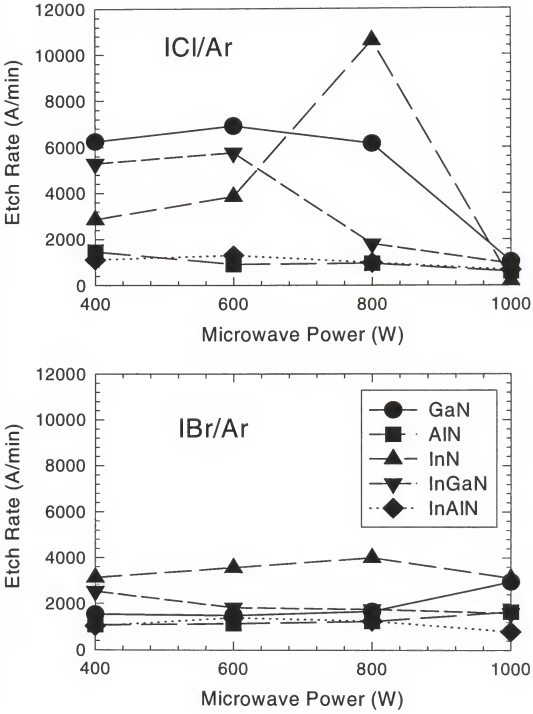

Figure 37. Etch rate as a function of microwave power for GaN, InN, InAlN, AlN and InGaN in 4 ICl/4 Ar (top) or 4 IBr/4 Ar (bottom) plasmas (150 W rf, 1.5 mTorr).

sensitivity to reactant density. It is expected that below that density the etch rate is reaction-limited and above it there is competition between the reactants that limits the etch rate. A similar trend is observed for InN in the IBr/Ar mixtures although the peak is not as distinct.

The etch rates for InAlN and AlN were again quite low in IBr based plasmas (Fig. 37, bottom). GaN had constant etch rates for powers between 400 W and 800 W in the IBr chemistry, and then increased sharply at 1000 W. The InGaN etch rate again decreased with increasing microwave power. As the InGaN etch rate increased monotonically with increasing rf power (as will be seen shortly), the removal of the etch products would seem to be limiting the etch rates for this material.

Figure 38 shows the etch rate as a function of rf power for GaN, InN, InAlN, AlN and InGaN in ICl/Ar (top) and IBr/Ar (bottom) plasmas for chuck powers between 50 and 250 W. Microwave power was held at 1000 W and the flow was held at 4 sccm ICl or IBr / 4 sccm Ar. The AlN and InAlN rates were affected very little by increasing rf power in either chemistry. GaN, InN and InGaN all have large increases in etch rate as the rf is increased from 150 to 250 W in the ICl chemistry. This could mean that the bombarding ions have enough energy to remove the less volatile etch product at this power or to more efficiently break bonds, allowing the

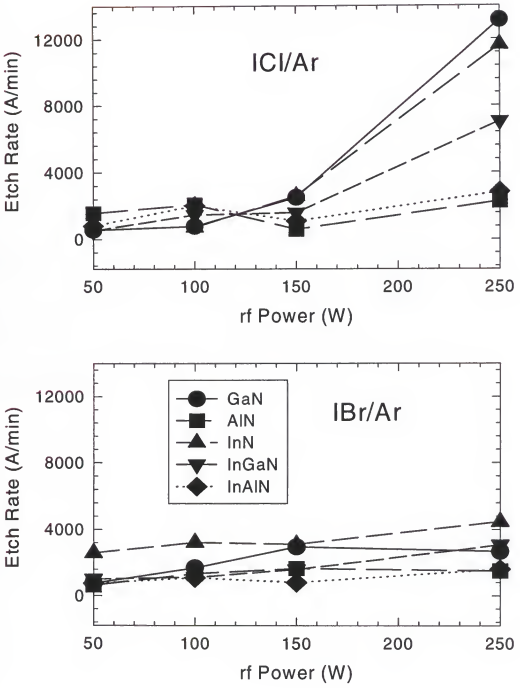

Figure 38. Etch rate as a function of rf power for GaN, InN, InAlN, AlN and InGaN in 4 ICl/4 Ar (top) or 4 IBr/4 Ar (bottom) plasmas (1000 W ECR, 1.5 mTorr).

etch to proceed with both I- and Cl- etch products. GaN etch rates in IBr/Ar increased with increased rf power to 150 W, and then decreased slightly at 250 W, where the sputtering ions may have removed reactants before the etch could proceed. InN and InGaN in IBr/Ar plasmas had large increases in etch rate as the rf was increased from 150 to 250 W, similar to the results in ICl/Ar.

In Fig. 39 the RMS roughness for GaN etched in ICl/Ar as a function of rf power is shown. The RMS roughness for the as-grown sample is shown for reference. These samples were unpatterned to avoid roughness caused by mask material being redeposited. The etched surfaces were found to be significantly smoother than that of the as-grown sample indicating that surface features are removed predominantly by sputtering, as mentioned earlier. Above 150 W the surface roughness begins increasing again, probably due to the onset of preferential sputtering.

AES depth profiles of GaN as-grown and etched in ICl/Ar at 50 W or 100 W rf power are shown in Fig. 40. At these powers no reduction in the N/Ga ratio. This means that there is little preferential loss of N during the etching at these powers. Adventitious C and O from native oxide are also observed on the surface of these samples. I and Cl are found in the top 25 Å of the etched samples. Similar results were found for GaN etched in IBr/Ar plasma, though no Br was

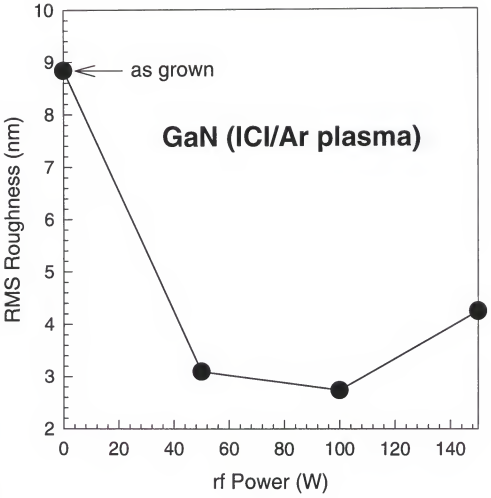

Figure 39. RMS roughness for GaN as a function of rf power in 4 ICl/4 Ar 1000 W ECR, 1.5 mTorr discharges plasmas.

detected on the surface. At high rf powers one would expect preferential N-loss, as reported previously by Shul et. al.[8]

Summary

The etch rates for GaN, InN, InAlN, AlN and InGaN were measured in ICl/Ar and IBr/Ar plasmas. The sensitivity to changes in plasma chemistry, microwave power and rf power appears to be directly influenced by the volatility of the group-III -I and Cl- or Br-etch products. InN, with the largest difference between volatility of etch products, proved to be the most sensitive to the plasma composition and ion density in ICl/Ar plasma chemistries. Very fast etch rates were achieved for GaN, InN and InGaN in ICl/Ar chemistries. At 250 W rf power AlN and InAlN had slow etch rates in this mixture and were affected very little by changes in etch conditions. GaN and AlN etched in IBr/Ar showed a sharp increase in etch rate as the IBr composition increased from 50 to 100 %, while the etch rates for the other materials stayed relatively constant above 25% IBr. All the materials showed a general increase in etch rate with increasing rf power in both chemistries. The etched surface of GaN under both plasma chemistries was found to be extremely smooth with little preferential loss of N from the surface at low rf powers. There was no detectable residue

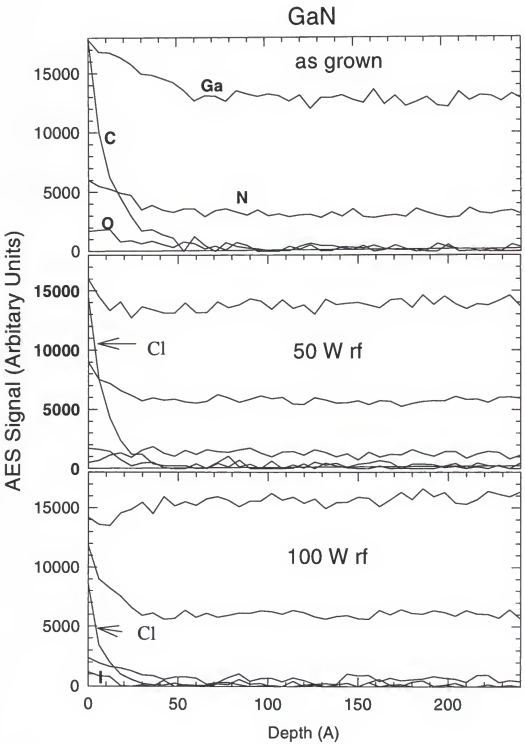

Figure 40. AES depth profiles of GaN as-grown (top), and etched in 4 ICl/ 4 Ar at 50 W rf (middle) and at 100 W rf (bottom) power. The ECR source power was 1000 W and the pressure 1.5 mTorr.

from the etch after IBr/Ar plasma, and only slight Cl residue in ICl/Ar chemistry.

Electron Cyclotron Resonance Plasma Etching Of AlGaN

A comparison of etch rates for GaN, $Al_{0.2}Ga_{0.8}N$, $Al_{0.31}Ga_{0.69}N$ and AlN was performed in Cl_2/Ar and BCl_3/Ar ECR plasmas. Growth was done at 76 Torr, at 1050 °C, on the basal plane of sapphire.[113] The precursors were trimethlygallium, trimethylaluminum and ammonia. The growth rate was relatively low (~0.7 μm/hr), and the layers were semi-insulating, with the density of deep compensating centers greater than the shallow donor concentration. The room temperature electron concentration was ~ 10^{11} cm^{-3} with a mobility of ~ 100 $cm^2/V\bullet s$. The thickness of the layers was approximately 1 μm.

Figure 41 shows the etch rate as a function of microwave power for BCl_3/Ar (top) and Cl_2/Ar (bottom) 10 sccm/5 sccm. For the BCl_3/Ar chemistry, there were decreasing etch rates with increasing microwave power for all compositions. This was probably due to increasing plasma density, which can cause the dc bias to decrease, lowering the ion energy. Because of the large bond strengths of these materials, ion sputtering and ion-assisted desorption of reacted species is necessary. It is also possible that with the increased density of sputtering ions, the reactant

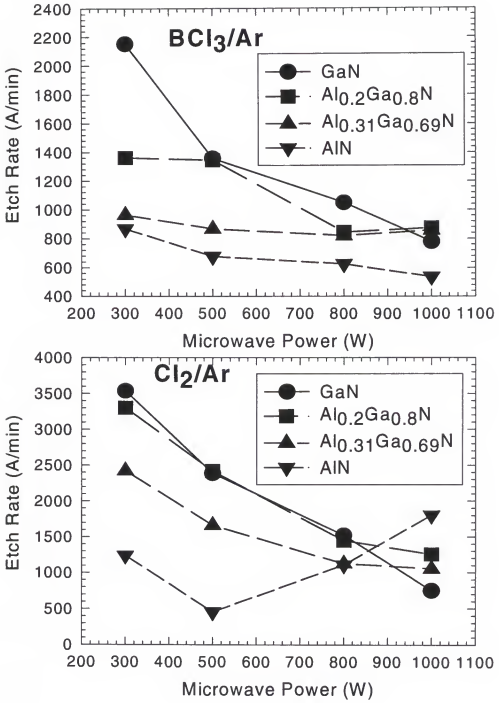

Figure 41. Etch rate as a function of microwave power for BCl_3/Ar (top) and Cl_2/Ar (bottom).

species may be sputter desorbed prior to reaction. The etch rates are quite low, and in general reflect the bond strength of the material. GaN showed the highest etch rate (2200 Å/min at 300 W microwave power), with the etch rate for $Al_xGa_{1-x}N$ decreasing as the composition of AlN increased.

The etch rates in the Cl_2/Ar chemistry were somewhat faster, Fig 41 (bottom), and followed a trend similar to that in the BCl_3/Ar chemistry. The etch rates decreased with increasing microwave power and increasing AlN composition, except for AlN above 500 W microwave power. AlN etched faster at 1000 W microwave power than any of the others. $AlCl_3$ is slightly more volatile than $GaCl_3$ and there is more active Cl available in the Cl_2 discharge.

Figure 42 shows the etch rate as a function of rf power for BCl_3/Ar (top) and Cl_2/Ar f power is increased from 50 W to 250 W, while AlN had a slight increase to 150 W and then remained constant. The etch rate of the AlGaN samples rose initial at 100W (x=0.31) or 150 W (x=0.2) and then decreased. This would indicate that the sputtering ions had enough energy to break the bonds in the GaN but not in the AlN, at higher energies. The ions initially sputter-desorb the reacted products, but as the power increases begin to sputter-remove species before they can react.

In the chlorine based etch, on the other hand, Fig 42 (bottom), the etch rates increased with increasing rf power

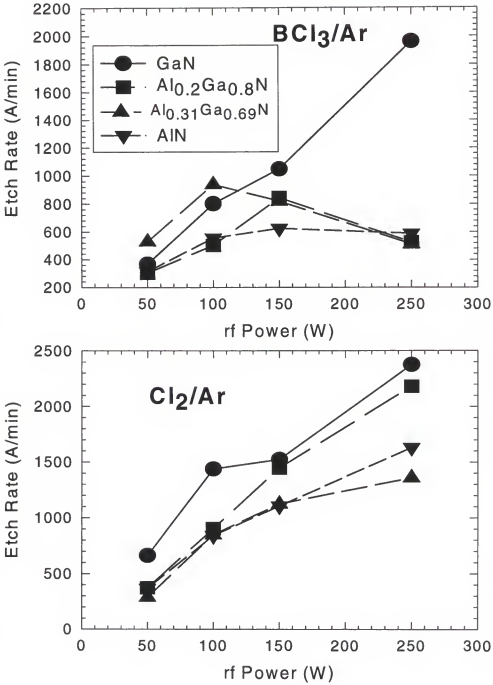

Figure 42. Etch rate as a function of rf power for BCl_3/Ar (top) and Cl_2/Ar (bottom).

for all sample compositions. There were more chlorine neutrals available in this chemistry which may have allowed it to proceed more rapidly. Once again GaN etched fastest over the range, with the etch rate decreasing in general with increasing AlN concentration.

Figure 43 shows the RMS roughness data for BCl_3/Ar (top) and Cl_2/Ar (bottom) as a function of rf power. The samples etched in Cl_2/Ar were in general smoother than those etched in BCl_3/Ar. This may have been due to the higher density of reactive neutrals in the chlorine discharges which produced a more optimized ratio of ions-to-Cl radicals. The maxima in the normalized RMS plots may be due to the onset of preferential sputtering of nitrogen from the surface, increasing surface roughness. As the rf power is further increased, the ions may have enough energy to remove the group III species as well.

The etch rates were quite low for these chemistries, The fastest rates being about 2000 Å/min for AlN, 2500 Å/min for $Al_{0.31}Ga_{0.69}N$ and 3400 Å/min for $Al_{0.2}Ga_{0.8}N$. Higher ion energies may be necessary to attain higher etch rates for these high bond strength materials. Further work is necessary to optimize the etch parameters.

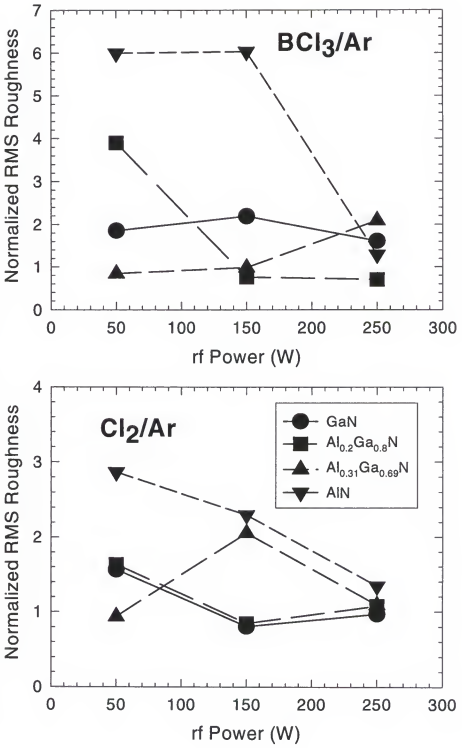

Figure 43. Normalized RMS roughness data for BCl_3/Ar (top) and Cl_2/Ar (bottom) as a function of rf power.

Selectivity

Heterostructures such as AlGaN/InGaN/GaN play an important role for nitride based devices, and the ability to stop an etch on a particular layer will determine how useful the etch processes are to manufacturing. It is important to have high selectivities while still maintaining a fast etch rate for the material.

Because of their high bond strengths, dry etches for the group III-nitrides generally require high rf powers under RIE conditions and high plasma densities under ECR conditions, in order to achieve practical rates. This tends to reduce the selectivity of an etch process due to the predominance of physical sputtering and hence the inability to form chemical etch-stop reactions. The bond strength of AlN and InAlN indicate that they will etch slower than the other group III-nitrides because of their high average bond energies. It should be possible to achieve acceptable selectivities for GaN, InN and InGaN over AlN and InAlN, and much more difficult to achieve the reverse. However, as discussed in the previous chapter, KOH-based wet etches for AlN and InAlN[63] are selective over GaN, InN and InGaN. This etch solution can be employed when a selective etch of AlN or InAlN over the other III-nitrides is necessary. Selectivities were calculated from etched performed in ECR and RIE plasma etching in various chemistries.

Figure 44 (top) shows the selectivity of InN or InGaN over GaN, and GaN over AlN with a $CH_4/H_2/Ar$ plasma chemistry under RIE conditions. The highest selectivity, ~ 4.5 was obtained for GaN/AlN. The selectivity decreased with increasing ion energy above 250 W (~-275 V dc self bias) for all the materials, to approximately unity at 450W rf power. At powers < 250 W the selectivity may have increased due to enhanced removal of the In and Ga etch products relative to the Al products.

Figure 44 (bottom) shows the selectivity with a $CH_4/H_2/Ar$ plasma chemistry under ECR (1000 W) conditions. At 50 W rf power InN was etched ~6.5 times faster than GaN, but the selectivity dropped sharply as the rf power was increased to 250 W. The InN bonds are weaker than those of GaN, and at low rf power the InN was etched faster. As the sputtering ion energy increased, the difference in etch rates decreased. Above 250 W the selectivity increased slightly to a value of 3 at 450 W, but there is preferential loss of N under these conditions, as determined by AES measurements. At 50 W rf, GaN is etched almost 4 times faster than AlN, but the selectivity again dropped rapidly with increasing rf power. There was no significant selectivity of GaN over InGaN under these conditions. The etch rates of the nitrides were up to an order of magnitude faster under ECR conditions than RIE conditions. The etch

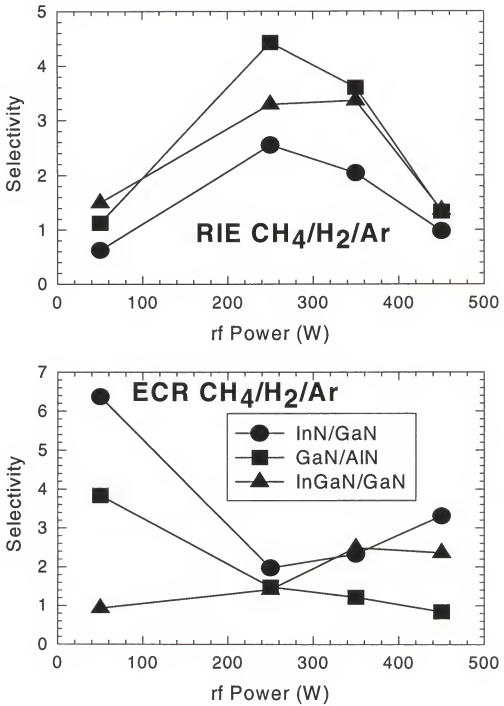

Figure 44. Selectivity of InN and InGaN over GaN, and GaN over AlN under RIE (top) and ECR (bottom) $CH_4/H_2/Ar$ plasma conditions as a function of rf power.

rates with this plasma chemistry under ECR conditions with 450 W rf power were ~1700 Å/min for GaN, 2000 Å/min for AlN, 3800 Å/min for InGaN and 5800 Å/min for InN.

The selectivity of GaN over InN, AlN or InGaN under RIE (top) and ECR (bottom) Cl_2/Ar plasma conditions is shown as a function of rf power in Fig. 45. Under RIE conditions there was a wide range of values. At low rf powers GaN was etched over 10 times faster than InGaN. The volatility of $GaCl_3$ is much higher than that of $InCl_3$ (boiling points of 201 °C and 600 °C respectively) so at low rf powers this predominates, while as the sputtering ion energy is increased the $InCl_3$ could be removed more easily. The same basic trends were obtained for GaN/InN. GaN's selectivity over AlN rose with increasing rf to a value of almost 9 at 450 W rf. The boiling points of $GaCl_3$ and $AlCl_3$ (183 °C) are similar, which indicated that it is the differential in bond strengths between GaN and AlN that is the dominant factor in this case. The ions may have gained enough energy to break much higher numbers of bonds in the GaN relative to those in AlN as the rf power increased.

Under ECR plasma conditions (1000W source power) the selectivities were generally lower. At 50 W rf the selectivity of GaN over AlN was ~ 11, but this dropped to a value of 4 as the rf was increased to 150 W and then remained constant. The values for GaN over InN and InGaN

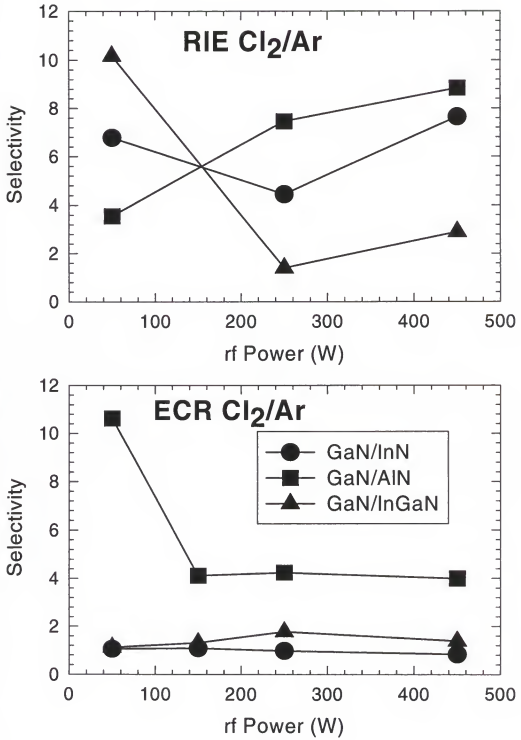

Figure 45. Selectivity of GaN over InN, AlN or InGaN under RIE (top) and ECR (bottom) Cl_2/Ar plasma conditions as a function of rf power.

were less than 2 for all rf powers. Due to the higher density of free radicals and the higher rate of reaction attempts, the etch rates for all nitrides are more similar under ECR conditions. The etch rates with this plasma chemistry under ECR conditions and 450 W rf power were ~ 6500 Å/min for GaN, 7800 Å/min for InN, 4700 Å/min for InGaN and 1600 Å/min for AlN.

Figure 46 shows the etch selectivity of GaN over InN, InAlN, InGaN or AlN in ICl/Ar discharges as a function of rf power (top), percent ICl (middle) and microwave power (bottom). The selectivity of GaN over the other nitrides rose with increasing rf power, with GaN/AlN reaching ~ 6 and GaN/InAlN almost 5 at 250 W rf. The volatility of the $InCl_3$ was lower than that of $GaCl_3$, and as the percent ICl in the etch increased, so did the selectivity for GaN/InN, reaching ~ 10 at 100% ICl. With both $GaCl_3$ and GaI_3 having high volatilities, with increasing reactant concentration, GaN was etched faster than the In-containing compounds, which may still be limited by removal of $InCl_3$. GaN etched much faster than AlN and InAlN as well for most microwave powers (Figure 46, bottom), achieving selectivities of ~8 and 5 respectively at 600 W microwave power. In IBr/Ar chemistries the selectivities were low, as shown in Fig. 47, never going above 4 for any set of rf or microwave powers of plasma compositions. This may be due to the similar volatilities of iodide and bromide etch products.

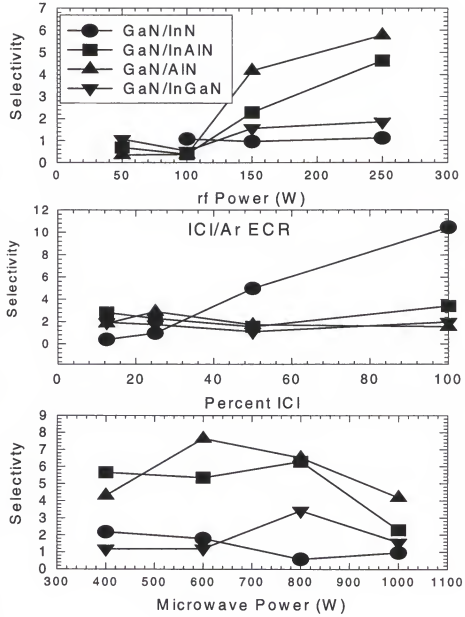

Figure 46. Selectivity of GaN over InN, InAlN, InGaN or AlN in ICl/Ar plasmas as a function of rf power (top), percent ICl (middle) and microwave power (bottom). The ECR power was 1000 W for the top two plots, the rf power 150 W for the bottom two plots and the plasma composition 4 ICl/4 Ar for the top and bottom plots.

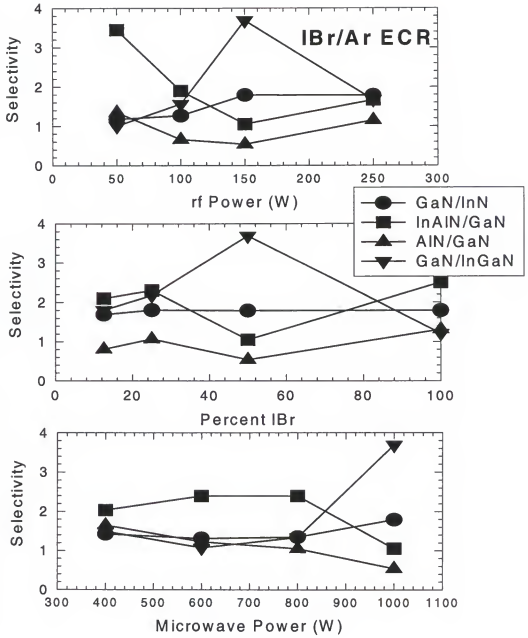

Figure 47. Selectivity of GaN over InN, InAlN, InGaN or AlN under IBr/Ar plasmas as a function of rf power (top), percent ICl (middle) and microwave power (bottom). The ECR power was 1000 W for the top two plots, the rf power 150 W for the bottom two plots and the plasma composition 4 ICl/4 Ar for the top and bottom plots.

In summary Cl_2-based etches appear to be the best choice for achieving the highest selectivities of GaN over InN, AlN, InAlN and InGaN. Relatively high selectivities of InN/GaN were achieved in $CH_4/H_2/Ar$ under ECR conditions at low rf powers. In order to attain selectivities of AlN and InAlN over GaN a wet etch based on a KOH solution may be necessary. Further investigations into the addition of other gases into the etch, such as SF_6, may lead to higher selectivities for these materials.

CHAPTER 7

THERMAL STABILITY OF OHMIC CONTACTS

Introduction

The III-Nitrides pose a problem in the development of low resistance ohmic contacts because of their wide bandgaps. Most of the work done in this area has been focused on n-type GaN. Au and Al single metal contacts to n^+ GaN and non- alloyed Au/Ti and Al/Ti were found to have contact resistances of ~ 10^{-3} to 10^{-4} $\Omega \cdot cm^2$.[16,34,114] Lin et. al.[36] reported the lowest contact resistance to n^+ GaN, with Ti/Al contacts after annealing at 900 °C for 30 sec in a rapid thermal annealer (ρ_c = $8x10^{-6}$ $\Omega \cdot cm^2$). They suggested the formation of a TiN interface as important in the formation of the low resistance contact. W was found to produce low resistance ohmic contacts to n^+ GaN (ρ_c ~ 10^{-6} $\Omega \cdot cm^2$) with little interaction between the semiconductor and the metal up to 800 °C.[117] WSi_x on GaN was found to be stable to 800 °C as well, with a contact resistance of ~10^{-5} $\Omega \cdot cm^2$.[118] Graded contacts to GaN have been formed with InN,[119] and InGaN with WSi_x.[43] Ohmic contacts to InN have also been investigated, with non-alloyed Ti/Pt/Au determined to form

ρ_c = 1.8×10^{-7} $\Omega \cdot cm^2$ contacts.[120] Graded $In_xGa_{1-x}As$/InN contacts have also been used on GaAs/AlGaAs heterojunction bipolar transistors, with ρ_c as low as 5×10^{-7} $\Omega \cdot cm^2$.[10]

For high temperature electronics applications, or for high reliability, it would be preferable to employ refractory metal contacts such as W and WSi_x. Moreover, the contact resistance could be reduced if lower bandgap In-containing alloys (or InN) were used as contact layers on GaN, much as the case with InGaAs on GaAs. However, the In-based nitrides are less thermally stable than GaN, and it is important to establish the trade off between better contact resistance and poorer temperature stability.

Experimental

W, $WSi_{0.44}$ and Ti/Al contacts deposited on n^+ $In_{0.65}Ga_{0.35}N$, n^+ InN and n^- $In_{0.75}Al_{0.25}N$ were investigated. The electrical, structural and chemical stability of these contacts were examined after anneals up to 900 °C, using Transmission Line Method (TLM) measurements, SEM and AES. Temperature dependent TLM measurements in the range -50 °C to 125 °C were used to obtain information about the conduction mechanism in these contact structures.

The InN, $In_{0.65}Ga_{0.35}N$ and $In_{0.75}Al_{0.25}N$ samples used were highly autodoped n-type (~10^{20} cm^{-3}, ~ 10^{19} cm^{-3} and 8×10^{18} cm^{-3} respectively) due to the presence of native defects. The

samples were rinsed in $H_2O:NH_4OH$ (20:1) for 1 min just prior to deposition of the metal to remove native oxides. The metal contacts were sputter deposited to a thickness of 1000Å in the case of W and $WSi_{0.44}$, and then etched in SF_6/Ar in a Plasma Therm reactive ion etcher (RIE) to create TLM patterns. [121,122] For the Ti/Al contacts, 200Å of Ti and then 1000Å of Al was deposited, and the TLM pattern formed by lift off. The nitride samples were subsequently etched in $Cl_2/CH_4/H_2/Ar$ in an Electron Cyclotron Resonance (ECR) etcher to produce the mesas for the TLM patterns.[98] The samples were annealed at temperatures from 300 to 900 °C for 15 sec under a nitrogen ambient in a RTA system (AG-410).

Results And Discussion

The contact resistance for W, WSi_x and Ti/Al ohmic contacts to InGaN as a function of annealing temperature is shown in Figure 48. All contacts had similar contact resistance as deposited, ~ $2\text{-}4x10^{-7}$ $\Omega \cdot cm^2$. Above 600 °C, the Ti/Al contacts degraded rapidly, and the WSi_x continued to degrade, while ρ_c for both samples increased up to ~ 10^{-5} $\Omega \cdot cm^2$ at 900 °C. The error in these measurements was estimated to be ±10 % due mainly to geometrical contact size effects. The widths of the TLM

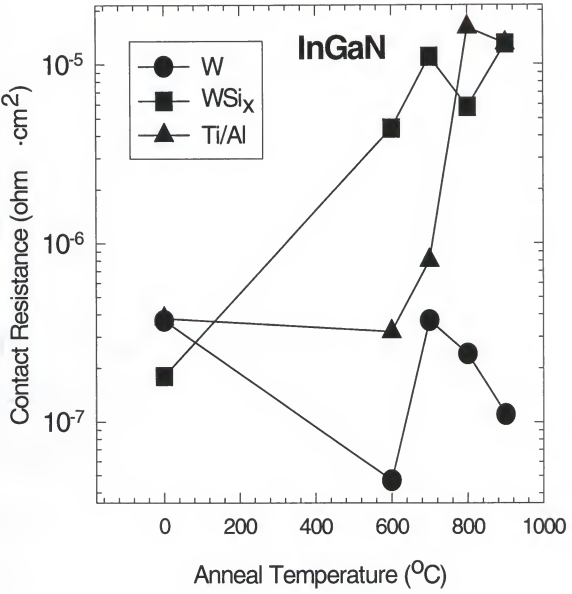

Figure 48. Contact resistance for W, $WSi_{0.44}$ and Ti/Al ohmic contacts to InGaN as a function of annealing temperature.

pattern spacings varied slightly due to processing, (maximum of ± 5 %) as determined by SEM measurements, which were taken into account when calculating the contact resistances.

Figure 49 shows SEM micrographs of W and Ti/Al contacts on InGaN as-grown and annealed. The W was still quite smooth even after 900°C anneal, while the Ti/Al had significant pitting at the lowest anneal of 500 °C even though the contact resistance did not degrade until ≥ 600 °C. AES showed the degradation was due to outdiffusion of In and N.

In Fig. 50 AES depth profiles of InGaN contacted with W before and after a 900 °C anneal are shown. As-deposited samples show some apparent diffusion of W into the sample but this is probably indicative of surfave roughness. After annealing however there was a large out-diffusion of In and N. The In has diffused about 500 Å into the W, showing a sharp peak in concentration at that position. Though much smaller amounts of N have diffused out, it also had a peak in concentration at that position. The Ga remained stable, consistent with results that found GaN to be stable with W to high temperatures.[116] There was no significant diffusion of W after annealing emphasizing the excellent thermal stability of these contacts.

The contact resistance for ohmic contacts of W, WSi_x and Ti/Al to InN as a function of annealing temperature is

Figure 49. SEM micrographs of W contacts on InGaN as-grown (top right) and annealed at 900 °C (top left), Ti/Al contacts on InGaN as-grown (bottom left) and annealed at 500 °C (bottom right).

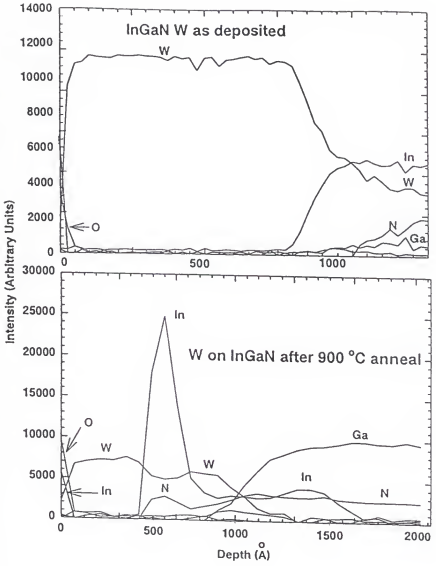

Figure 50. AES depth profiles of InGaN contacted with W before (top) and after a 900 °C anneal (bottom).

shown in Fig. 51. As-deposited samples had similar contact resistances to InGaN, indicating a similar conduction mechanism. WSi_x contacts showed the most degradation at low temperature, with the resistance rising a factor of 5 after 300 °C annealing and then remaining constant. Ti/Al deviated little from initial values, although there was severe pitting on samples annealed at 500 °C (Figure 49, bottom) while W resistance began to degrade at 500 °C.

In Fig. 52 the contact resistance is shown for W, WSi_x and Ti/Al ohmic contacts to InAlN as a function of annealing temperature. As-deposited Ti/Al had the lowest contact resistance on this material, ρ_c ~$1x10^{-4}$ $\Omega \cdot cm^2$. W had the highest initial contact resistance, (ρ_c ~ $1x10^{-2}$ $\Omega \cdot cm^2$). The contacts showed morphological stability to 400 °C (Ti/Al) to 800 °C (W).

SEM micrographs of InAlN contacted with W, WSi_x and Ti/Al as-grown and annealed at 800, 700 and 400 °C respectively are shown in Fig. 53. The W on InAlN remained smooth until 800 °C, and then begins to form hillocks, as did the WSi_x contact at 700 °C. The Ti/Al began pitting at 400 °C. As will be seen in subsequent figures, the pitting in the Ti/Al contacts was due to diffusion of the Al through

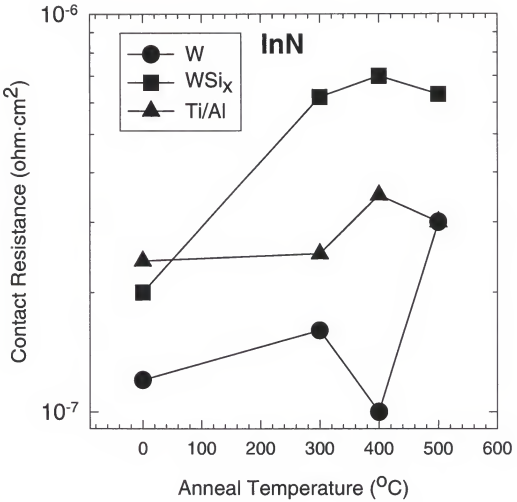

Figure 51. Contact resistance for ohmic contacts of W, WSi_x and Ti/Al to InN as a function of annealing temperature.

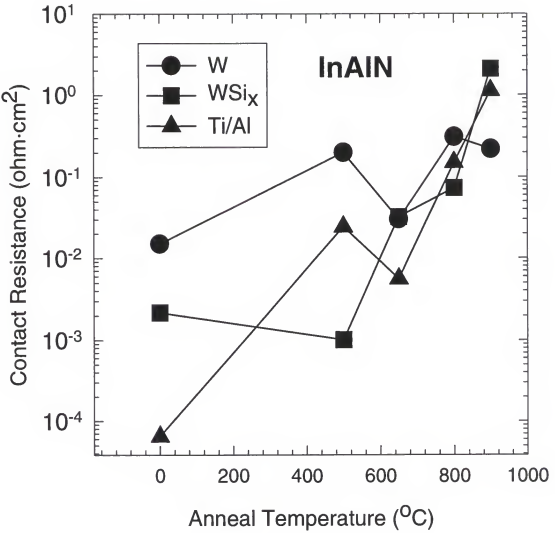

Figure 52. Contact resistance for W, WSi_x and Ti/Al ohmic contacts to InAlN as a function of annealing temperature.

the Ti into the sample. Hillocks appear to be formed from diffusion of In from the nitride sample into the contact layer.

Figure 54 shows the theoretical curves for contacts to InGaN of this doping level exhibiting thermionic, thermionic field, or field emission as their dominant conduction mechanisms. The curves are shown only to give the expected temperature dependence of ρ_c and the magnitude of the specific contact resistance is arbitrary. The theoretical values are calculated from[123]

$\rho_c \propto \exp(\Phi_b/E_{00})$ for field emission

$\rho_c \propto \exp[\Phi_b/E_{00}\coth(qE_{00}/kT)]$ for thermionic field emission

$\rho_c \propto \exp(q\Phi_b/kT)$ for thermionic emission

where

$$E_{00} = h/4\pi[N_d/m^*\varepsilon_s]^{1/2}$$

with Φ_b being the barrier height, N_d the donor concentration in the semiconductor, m* the effective mass of electrons in the material and ε_s the permittivity of the semiconductor. For field emission $qE_{00}/kT \gg 1$, for thermionic field emission $qE_{00}/kT \sim 1$, and for thermionic emission $qE_{00}/kT \ll 1$, with $q/kT \cong 0.026$ eV at 300 K. A fixed barrier height (1 eV) was assumed for calculations of the three conduction

Figure 53. SEM micrographs of InAlN contacted with W(top), WSi_x (middle) and Ti/Al (bottom) as-grown and annealed at 800, 700 and 400 °C respectively.

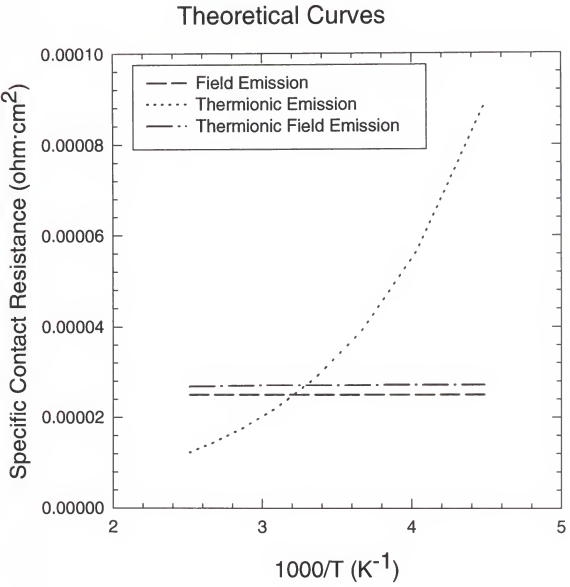

Figure 54. Theoretical curves for the temperature dependence of specific contact resistance of contacts in which thermionic emission, thermionic field emission, or field emission are the dominant conduction mechanism.

mechanisms, as other III-V semiconductors have pinned Fermi levels due to the presence of high densities of surface states. As values have not been definitively established for m^* and ε_s for all the nitride compounds, the best available values for InN were used, ($m^* = 0.1m_e$ and $\varepsilon_s = 8\varepsilon_o$).[44]

Over the temperature range studied there was little difference between the slope expected for the theoretical field emission and thermionic field emission plots (Figure 54). The thermionic field emission does have a slight upward slope with increasing reciprocal temperature, but it is less than the error found in the experimental measurements on the samples. By contrast, the thermionic emission case shows an obvious trend over the temperature range.

Temperature dependent contact resistance values for InGaN contacted with W and WSi_x are shown in Fig. 55. The specific contact resistance is very low ($< 10^{-5}\ \Omega \cdot cm^2$) for both metals. There is no clear pattern to the data over this temperature range. There is however no upward trend that would indicate thermionic emission. For this material, the value of E_{00} was estimated to be 0.63 eV based on doping levels. This gives a value of $qE_{00}/kT \sim 24$ indicating field emission conduction is expected to be dominant.

Figure 56 (top) shows the temperature dependent contact resistance data for InN contacted with WSi_x. The 500 °C annealed contact has approximately constant contact

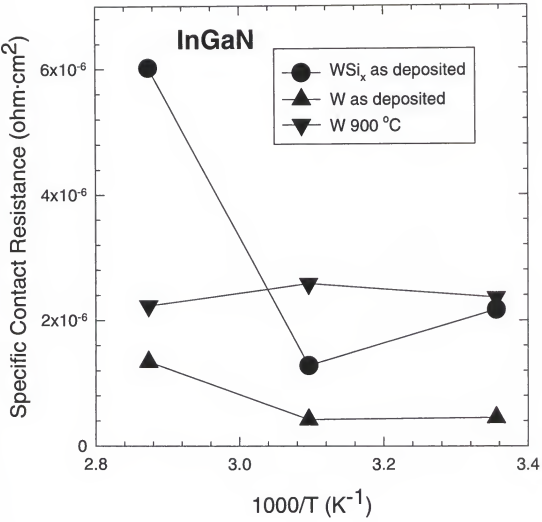

Figure 55. Experimentally measured, temperature-dependent specific contact resistance values for InGaN contacted with W and WSi_x.

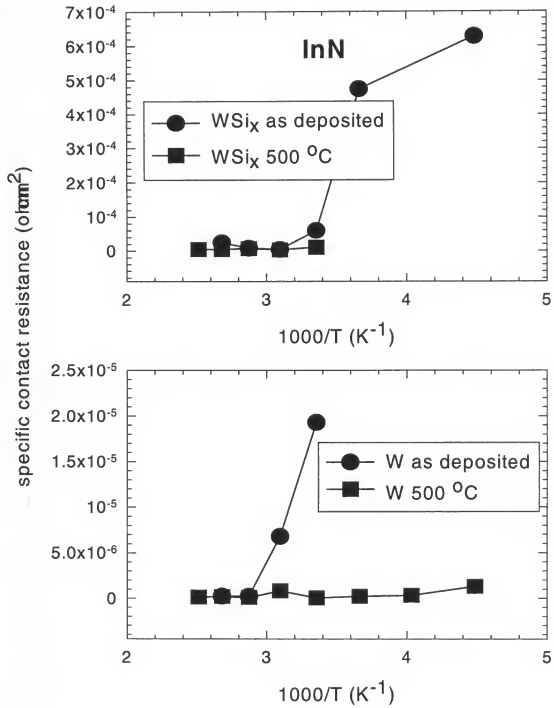

Figure 56. Experimentally determined, temperature-dependent specific contact resistance values for InN contacted with WSi_x (top) and W (bottom).

resistance over this temperature range, as is expected for InN with this doping level ($qE_{00}/kT \sim 77$). The contact resistance for the as-deposited contact, however, rises with temperature, characteristic of thermionic emission. This may be a result of changing doping levels in the InN because of the sputter deposition of the contact, as is the case for GaAs. In comparing the data in Fig. 55 and 56 it is seen that contacts to InN are more sensitive to temperature than InGaN. The specific contact resistance of InN contacted with W as deposited and after a 500 °C anneal was also measured (Fig. 56, bottom). Again the annealed contact shows a relatively constant contact resistance over the range while the as-deposited contact shows an upward trend.

Conclusion

W, WSi_x and Ti/Al were found to produce low resistance ohmic contacts on n^+ InGaN and InN. W contacts proved to be the most stable, and also gave the lowest resistance to InGaN and InN, $\rho_c < 10^{-7}\ \Omega\cdot cm^2$ after 600 °C anneal, and $1x10^{-7}\ \Omega\cdot cm^2$ after 300 °C anneal, respectively. Significant diffusion of In, N and Al, as well as Ti and W were found after anneal. The contact resistance stability varies for each material and degraded at temperatures > 400 °C on InN, ≥ 500 °C on InAlN and ≥ 600 °C on InGaN. W contacts remained

smooth at the highest anneal temperatures. Theoretical calculations based on the doping levels of InGaN and InN indicate that the dominant conduction mechanism in W-based ohmic contacts to these materials should be field emission. The experimental data fit curves for field emission or thermionic field emission for InGaN contacted with WSi_x and W. InN samples contacted with both W and WSi_x showed similar behavior after annealing at 500 °C, while for as-deposited the curves fit better to the thermionic emission case. This may indicate that the deposition of the contact metal lowered the doping levels in the InN, while annealing returned them to a higher level.

CHAPTER 8

CONCLUSION

Many processing techniques are needed to produce high performance, reliable III-V nitride based photonic and electronic devices. High temperature annealing is required in many of these processing steps, including maximization of implant isolated regions, activation of implanted ions or high temperature alloying of metal contacts. Ensuring that surface degradation of the III-V nitrides does not occur during these high temperature anneals is critical to device performance. The surface stability of AlN, GaN, InN, InAlN and InGaN was examined under rapid thermal annealing conditions, and it was found that the preferential loss of N from the surface is the most significant surface degradation mechanism. AlN and GaN were stable to 1000 °C, InGaN and InAlN to 800 °C and InN to 600 °C

Semi-insulating regions were formed in initially n- or p-type GaN using multiple energy N^+ implantation, and in $In_xAl_{1-x}N$ and $In_xGa_{1-x}N$ implanted with multiple energy N^+ ions and subsequently annealed up to 900 °C. Sheet resistances of $\geq 5\times10^9$ $\Omega/$ for N^+ implanted GaN, and $> 10^8$ $\Omega/$ were

obtained for N^+ implanted InAlN. In InGaN, sheet resistances typically 50-100 times higher than the as-grown values were obtained using N^+ implantation. In addition, n- and p-type doping of ion implanted species in GaN was obtained. Carrier activation percentages of 93% were obtained for Si which created n-type GaN and 62% for Mg, which when with co-implantated with P^+ producing p-type GaN.

Wet chemical etching of AlN and $In_xAl_{1-x}N$ in KOH based solutions was studied as a function of etch temperature, crystal quality and In composition. A peak occurs in the etch rate of InAlN at ~ 36 % InN, presumably due to competing mechanisms between decreasing bond strength and decreasing chemical sensitivity with increasing InN composition. The etches are diffusion controlled.

Dry etching of the nitrides was investigated under ECR and RIE conditions in Cl_2/Ar and CH_4/H_2/Ar discharges. A comparison of RIE and ECR etching of GaN, AlN, InN and InGaN in Cl_2/Ar and CH_4/H_2/Ar plasmas using the same reactor and etch conditions was performed. Etch rates up to an order of magnitude faster were measured under ECR conditions. ECR etching of GaN, InN, InAlN, AlN and InGaN in two new chemistries, ICl/Ar and IBr/Ar, was also examined, under various plasma compositions, microwave powers and rf powers. The GaN, InN and InGaN etch rates reached ~ 13000 Å/min, 11500 Å/min and ~7000 Å/min respectively at 250 W rf and

1000 W microwave power in ICl/Ar plasma discharges. These are the fastest yet reported for these materials. The etched surface of GaN was found to be smooth with no significant loss of N from the surface at low rf powers. The selectivities of etch for AlN, InAlN, InGaN and InN with respect to GaN were found to be generally low. The highest selectivities were found in Cl based etches, with values up to a factor of 10.

Finally, W, WSi_x and Ti/Al were found to produce low resistance ohmic contacts on n^+ InGaN and InN. W contacts proved to be the most stable, and also gave the lowest resistance to InGaN and InN, $\rho_c < 10^{-7}\ \Omega\cdot cm^2$ after 600 °C anneal, and $1x10^{-7}\ \Omega\cdot cm^2$ after 300 °C anneal, respectively. The dominant conduction mechanism was examined and is primarily field emission for InGaN and InN.

The key results obtained were:

(i). Identified the rate-limiting step in dry etching of nitrides, i.e. the initial bond breaking that allows volatile products to form, and exploited high ion flux ECR discharges to achieve the fastest etch rates ever obtained for the nitrides.

(ii). Development of a new plasma etch chemistry, ICl/Ar, based on an analysis of the volatility of the expected etch products, and showed that it produces very high etch rates.

(iii). Identified the implant isolation mechanism in GaN, InGaN and InAlN (damage-induced compensation) and measured the energy level of the defects responsible for the compensation.

(iv). Established the thermal stability limits during rapid thermal processing of GaN, AlN, InN, InAlN and InGaN, and identified N loss from the surface as the predominant surface degradation mechanism.

(v). Found the first wet solution (KOH) for InAlN alloys, measured the effect of material quality, composition and doping, and identified the rate-limiting step.

(vi). Developed thermally stable, low resistance ohmic contacts to In-containing nitrides and established the trade-off between lower ρ_c and poorer thermal stability at high In contents.

Future work will need to examine creation of low resistance contacts to p-type nitrides, p-dopant species with smaller ionization energies than Mg, improved plasma chemistries for achieving high selectivities and continue the search for wet etch solutions for the nitrides.

LIST OF REFERENCES

1. S. Strife and H. Morkoc, J. Vac. Sci. Technol B **10** 1237 (1992).

2. S. Nakamura, T. Mukai and M. Senoh, Appl. Phys. Lett. **64** 1687 (1994).

3. J.M. Gaines, R.R. Drenten, K.W. Haberern, T. Marshall, P. Mensz and J. Petruzzello, Appl. Phys. Lett. **62** 2462 (1993).

4. M.A. Haase, J. Qui, J.M. DePuydt and H. Cheng, Appl. Phys. Lett. **59** 1272 (1991).

5. R.M. Park, M. Troffler, C.M. Rouleau, J.M. Depuydt and M.A. Haase, Appl. Phys. Lett. **57** 2127 (1990).

6. H. Morkoc, S. Strite, G.B. Gao, M.E. Lin, B. Sverdlov and M. Burns, J. Appl. Phys. **76** 1363 (1994).

7. J.W. Palmour, C.H. Carter, C.E. Weitzel and K.J. Nordquist, Proc. Mat. Res. Soc. Symp. **339** 15 (1994).

8. F.A. Ponce, J.S. Major, W.E. Plano and D.F. Welch, Appl. Phys. Lett. **65** 2302 (1994).

9. M.A. Khan, D.J. Olson and J.N. Kuznia, Appl. Phys. Lett. **65** 64 (1994).

10. R.J. Molnar and T.D. Moustakas, J. Appl. Phys. **76** 4587 (1994).

11. R F. Davis, Proc. IEEE **79** 702 (1991).

12. R.F. Davis, J.W. Palmour and J.A. Edmond, IEDM pp 785-788 (1990).

13. T.P. Chow and R. Tyagi, IEEE Trans. Electron. Dev. **41** 1481 (1994).

14. I. Akasaki and H. Amano, J. Electrochem. Soc. **141** 2266 (1994).

15. J.I. Pankove, Mat. Res. Soc. Symp. Proc. **162** 515 (1990).

16. S. Nakamura, M. Senoh, and T. Mukai, Jpn. J. Appl. Phys. Lett. **30** L1708 (1991).

17. I. Akasaki, H. Amano, M. Kito, and K. Kiramatsu, Lumin. **48/49** 666 (1991)

18. S.Nakamura, M. Senoh, S. Nagahama, N. Iwasa, T. Yamada, H. Kiyokvand and Y. Sugimoto, Jpn. J. Appl. Phys. **35** L74 (1996).

19. S. Nakamura, M. Senoh, S. Nagahama, N. Iwasa, T. Yamada, T. Matsushita, Y. Sugimoto, H. Kiyoku, Applied Physics Letters **69** 1477-1479 (1996).

20. S. Nakamura presented at Oyo Butsuri Conference in Japan and at the Optoelectronics and Communications COnference (OECC) in Chiba, Japan, (July 1996).

21. "Toshiba Blue GaN Laser" press-released Sept 11,1996 in Japanese, and submitted to JJAP.

22. T Egawa, H Ishikawa, T Jimbo, M Umeno, Applied Physics Letters **69** 830-832 (1996).

23. M Osinski, J Zeller, PC Chiu, BS Phillips, DL Barton, Applied Physics Letters **69** 898-900 (1996).

24. S.C. Binari, L.B. Rowland, W. Kruppa, G. Kelner, K. Doverspike and D.K. Gaskill, Electron. Lett. **30** 1248 (1994).

25. M.A. Khan, J.N. Kuznia, A.R. Bhattarai and D.T. Olson, Appl. Phys. Lett. **62** 1248 (1993).

26. M.A. Khan, M.S. Shur, and Q. Chen, Electron. Lett. **31** 2130 (1995).

27. M.A. Khan, J.N. Kuznia, D.T. Olson, W. Schaf, J. Burm and M.S. Shur, Appl. Phys. Lett. **65** 1121 (1994).

28. M.A. Khan, M.S. Shur, J.N. Kuznia, J. Burm and W. Schaff, Appl. Phys. Lett. **66** 1083 (1995).

29. M.A. Khan, Q. Chen, C.J. Sun, J.W. Wang, M. Blasingame, M.S. Shur and H. Park, Appl. Phys. Lett. **68** 514 (1996).

30. W. Kruppa, S.C. Binari and K. Doverspike, Electon. Lett. **31** 1951 (1995).

31. S.C. Binari, L.B. Rowland, G. Kelner, W. Kruppa, H.B. Dietrich, K. Doverspike and D.K. Gaskill, Inst. Phys. Conf. Ser. **141** 459 (1995).

32. Q Chen, MA Khan, JW Yang, CJ Sun, MS Shur, H Park, Applied Physics Letters **69**, 794-796 (1996).

33. C.R. Abernathy, J. Vac. Sci. Technol. A **11** 869 (1993).

34. C.R. Abernathy, Mat. Sci. Eng. Rep. **14**, 203 (1995).

35. S. Nakamura, M. Senoh, and T. Mukai, Appl. Phys. Lett. **62** 2390 (1993).

36. M.E. Lin, Z. Ma, F.Y. Huang, Z.F. Fan, L.H. Allen and H. Morkoc, Appl. Phys. Lett. **64**, 1003 (1994).

37. J.S. Foresi and T.D. Moustakas, Appl. Phys. Lett. **62**, 2859 (1993).

38. T. Matsuoka, H. Tanaka, T. Sasaki and A. Katsui, Inst. Phys. Conf. Ser. **106**, 141 (1990).

39. M.E. Lin, B.N. Sverdlov and H. Morkoc, Appl. Phys. Lett. **63**, 3625 (1993).

40. C.B. Vartuli, S.J. Pearton, C.R. Abernathy, J.D. MacKenzie and J.C. Zolper, J. Vac. Sci. Technol. B, **13**, 2293 (1995).

41. J.C. Zolper, S.J. Pearton, C.R. Abernathy and C.B. Vartuli, Appl. Phys. Lett. **66**, 3043 (1995).

42. S.J. Pearton, C.B. Vartuli, J.C. Zolper, C. Yuan and R.A. Stall, Appl. Phys. Lett. **67**, 1435 (1995).

43. F. Ren, C.R. Abernathy, S.N.G. Chu, J.R. Lothian and S.J. Pearton, Appl. Phys. Lett. **66**, 1503 (1995).

44. L.L. Smith and R.F. Davis, in Properties of Group III Nitrides, ed. J.H. Edgar (INSPEC, Stevenage, UK 1994).

45. S. Porowski and I. Grzegory, in Properties of Group III Nitrides, ed. J.H. Edgar (INSPEC, Stevenage, UK 1994).

46. G.A. Slack and T.F. McNelly, J. Cryst. Growth **34**, 263 (1976).

47. J. Pasternak and L. Roskovcova, Physica Status Solidi, **7**, 331 (1964).

48. J.A. Van Vechten, Phys. Rev. B **7**, 1479 (1973).

49. J. Karpinski, J. Jun and S. Porowski, J. Cryst. Growth **66**, 1 (1984).

50. R. Madar, G. Jacob, J. Hallais and R. Fruchart, J. Cryst. Growth **31**, 197 (1975).

51. C.D. Thermond and R.A. Logan, J. Electrochem. Soc. **119**, 622 (1972).

52. J.B. MacChesney, P.M. Bridenbaugh and P.B. O'Connor, Mater. Res. Bull. **5**, 783 (1970).

53. R.D. Jones and K. Rose, J. Phys. Chem. Solids **48**, 587 (1987).

54. A.M. Vorobev, G.V. Evseeva and L.V. Zenkevich, Russ. J. Phys. Chem. **47**, 1616 (1973).

55. J.C. Zolper, M. Hagerott-Crawford, A.J. Howard, J. Rainer and S.D. Hersee, Appl. Phys. Lett. **68**, 200 (1996).

56. S.J. Pearton and R.Caruso, J. Appl. Phys. **66**, 663 (1989).

57. H.P. Marsuka, and J.J. Tietjen, Appl. Phys. Lett. **15**, 327 (1969).

58. R. Groh, G. Gerey, L. Bartha and J.I. Pankove, Phys. Stat. Solidi A **26**, 363 (1974).

59. C.R. Abernathy, J.D. MacKenzie, R.J. Shul, A. Howard and J.S. Williams, Electrochem. Soc. Proc. Vol **95-21** 1 (1995).

60. R.J. Mileham, S.J. Pearton, C.R. Abernathy, J.D. MacKenzie, R.J. Shul and S.P. Kilkoyne, Appl. Phys. Lett. **67**, 1119 (1995).

61. J.G. Kim, A.C. Frenkel, H. Liu and R.M. Park, Appl. Phys. Lett. **65** 91 (1994).

62. S. Nakamura, T. Mukai and M. Senoh, Jap. J. Appl. Phys. **31** 2883 (1992).

63. H. Amano, M. Kito, K. Hiramatsu and I. Akasaki, Jap. J. Appl. Phys. **28** L 2112 (1989).

64. M.E. Lin, G. Xue, G.L. Zhou, J.E. Greene and H. Morkoe, Appl. Phys. Lett. **63** 932 (1993).

65. B. Goldenberg, J.D. Zook and R.J. Ulmer, Appl. Phys. Lett. **62** 381 (1993).

66. M. Rubin, N. Newman, J.S. Chan, T.C. Fu and J.T. Ross, Appl. Phys. Lett **64** 64 (1994).

67. C. Wang and R.F. Davis, Appl. Phys. Lett. **63** 990 (1993).

68. C.R. Abernathy, J.D. MacKenzie, S.J. Pearton and W.S. Hobson, Appl. Phys. Lett. **66** 1969 (1995).

69. J.I. Pankove and J.A. Hutchby, J. Appl. Phys. **47** 5387 (1976).

70. H.P. Maruska and J.J. Tiefjen, Appl. Phys. Lett. **15** 327 (1969).

71. R.G. Wilson, R.N. Schwartz. C.R. Abernathy, S.J. Pearton, N. Newman, M. Rubin, T. Fu and J.M. Zavada, Appl. Phys. Lett. **65** 992 (1994).

72. R.G. Wilson, J.M. Zavada, C.R. Abernathy, and S.J. Pearton, Appl. Phys. Lett. **66** 2238 (1995).

73. S.C. Binari, L.B. Rowland, G. Kelner, W. Kruppa, H.B. Dietrick, K. Doverspike and D.K. Gaskill, Proc. 1994 Int. Symp. Comp. Semicond., held in San Diego CA, Sept 1994.

74. S.J. Pearton, C.R. Abernathy, P.W. Wisk, W.S. Hobson and F. Ren, Appl. Phys. Lett. **63** 1143 (1993).

75. S.J. Pearton, Mat. Sci. Rep. **4** 313 (1991).

76. J.C. Zolper, A.G. Baca and S.A. Chalmers, Appl. Phys. Lett. **62** 2536 (1993).

77. M.V. Rao, S.M. Gulwadi, S. Mulpuri, D.S. Simons, P.H. Chi, C. Laneau, W.P. Hong, O.W. Holland and H.B. Dietrich, J. Electron. Mater. **21** 923 (1992).

78. J.P. Donnelly and C.E. Hurwitz, Solid State Electron. **21** 475 (1978).

79. S.J. Pearton, M.P. Ianuzzi, C.L. Reynolds, Jr. and L. Peticolas, Appl. Phys. Lett. **52** 395 (1988).

80. J.C. Zolper, M.E. Sherwin, A.G. Baca and R.P. Schneider, Jr., J. Electron. Mater. **24** 21 (1995).

81. J. Neugebarger and C.G. Van de Walle, Phys. Rev. B **50** 8067 (1994).

82. K.M. Taylor and C. Lenie, J. Electrochem. Soc. **107** 308 (1960).

83. Long and L.M. Foster, J. Am. Ceram. Soc. **42** 53 (1959).

84. N.J. Barrett, J.D. Grange, B.J. Sealy and K.G. Shephens, J. Appl. Phys. **57** 5470 (1985).

85. C.R. Aita and C.J. Gawlak, J. Vac. Sci. Technol. A **1** 403 (1983).

86. G.R. Kline and K.M. Lakin, Appl. Phys. Lett. **43** 750 (1983).

87. T. Pauleau, J. Electrochem. Soc. **129** 1045 (1982).

88. T.Y. Sheng, Z.Q. Yu and G.J. Collins, Appl. Phys. Lett. **52** 576 (1988).

89. Q.X. Guo, O. Kato and Y. Yoshida, J. Electrochem. Soc. **139** 2008 (1992).

90. J.C. Zolper, D.J. Reiger, A.G. Baca, S.J. Pearton, J.W. Lee, R.A. Stall, Appl. Phys. Lett. (in press).

91. I. Adesida, A. Mahajan, E. Andideh, M. Asif Khan, D.T. Olsen and J.N. Kuznia, Appl. Phys. Lett. **63** 2777.

92. M.E. Lin, Z.F. Zan, Z. Ma, L.H. Allen and H. Morkoc, Appl. Phys. Lett. **64** 887 (1994).

93. A.T. Ping, I Adesida, M. Asif Khan and J.N. Kuznia, Electron. Lett. **30** 1895 (1994).

94. H. Lee, D.B. Oberman and J.S. Harris, Jr., Appl. Phys. Lett. **67** 1754 (1995).

95. S.J. Pearton, C.R. Abernathy, F. Ren, J.R. Lothian, P.W. Wisk, A. Katz and C. Constantine, Semicond. Sci. Technol. **8** 310 (1993).

96. S.J. Pearton, C.R. Abernathy and F. Ren, Appl. Phys. Lett. **64** 2294 (1994).

97. L. Zhang, J. Ramer, K. Zheng, L.F. Lester and S.D. Hersee, MRS Fall Meeting, Boston MA, (1995).

98. R.J. Shul, S.P. Kilcoyne, M. Hagerott Crawford, J.E. Parmeter, C.B. Vartuli, C.R. Abernathy and S.J. Pearton, Appl. Phys. Lett. **66** 1761 (1995).

99. R.J. Shul, presented at 189th ECS meeting, Los Angeles CA, May 1996.

100. Properties of Group III Nitrides, ed. J.H. Edgar (INSPEC, London 1994).

101. CRC Handbook of Chemistry and Physics (CRC Press, Boca Raton, FL 1990).

102. S.J. Pearton, Int. J. Mod. Phys., B**8** 1781 (1994).

103. S.J. Pearton, C.R. Abernathy, F. Ren, and J.R. Lothian, J. Appl. Phys. **76** 1210 (1994).

104. S.J. Pearton, U.K. Chakrabarti, A.P. Kinsella, D. Johnson and C. Constantine, Appl. Phys. Lett. **56** 1424 (1990).

105. C.W. Krueger, C.A. Wang, D.Hsieh and M. Flytzani-Stepanopoulos, J. Cryst.Growth **153** 81 (1995).

106. C.W. Krueger, C.A. Wang and M. Flytzani-Stepanopoulos, Appl. Phys. Lett. **60** 1459 (1992).

107. D.C. Flanders, L.D. Pressman and G. Pinelli, J. Vac. Sci. Technol. B **8** 1990 (1990).

108. G.F. Doughty, S. Thomas, V. Law and C.D.W. Wilkinson, Vacuum **36** 803 (1986).

109. S.J. Pearton, U.K. Chakrabarti, A. Katz, F. Ren and T.R. Fullowan, Appl. Phys. Lett. **60** 838 (1992).

110. S.J. Pearton, U.K. Chakrabarti, W.S. Hobson, C.R. Abernathy, A. Katz, F. Ren, T.R. Fullowan, and A.P. Perley, J. Electrochem. Soc. **139** 1763 (1992).

111. C.W. Krueger, C.A. Wang and M. Flytzani-Stepanopoulos, Appl. Phys. Lett. **60** 1459 (1992).

112. W.A. Harrison, Electronic Structures and Properties of Solids (Freeman, San Francisco, 1980).

113. M. Shin, A.Y. Polyakov, M. Skowronski, D.W. Greve, R.G. Wilson, J.A. Freitas, to be published in the Proceedings of the Spring MRS Meeting, 1996, Symp E, also A.Y. Polyakov, M. Shin, D.W. Greve, M. Skowronski and R.G. Wilson, to appear in MRS Internet Journal of Nitride Semiconductor Research, 1996.

114. J.S. Forsei and T.D. Moustakas, Appl. Phys. Lett. **62** 2859 (1993).

115. M.A. Khan, T.N. Kuznia, A.R. Bhattaraia and D.T. Olson, Appl. Phys. Lett. **62** 1786 (1993).

116. S. Nakamura, M. Senoh and T. Mukai, Appl. Phys. Lett. **62** 2390 (1993).

117. M.W. Cole, D.W. Eckart, T. Monahan, R.L. Pfeffer, W.Y. Han, F. Ren, C.Yuan, R.A. Stall, S.J. Pearton, Y. Li and Y. Lu, J. Appl. Phys. (in press).

118. A. Durbha, "Study of Ohmic Contacts on Gallium Nitride Thin Films" Master thesis.

119. M.E. Lin, F.Y. Huang and . Morkoe, Appl. Phys. Lett. **64** 2557 (1994).

120. F. Ren, C.R. Abernathy, S.J. Pearton and P.W. Wisk, Appl. Phys. Lett. **64** 1508 (1994).

121. R.J. Shul, D.J. Rieger, A.G. Baca, C. Constantine and C. Barratt, Electron. Lett. **30** 85 (1994).

122. R.J. Shul, M.E. Sherwin, A.G. Baca and D.J. Rieger, Electron. Lett. **32** 70 (1996).

123. A.Y.C. Yu, Solid State Electron, **13** 239 (1970).

BIOGRAPHICAL SKETCH

Catherine B. Vartuli graduated from the State University of New York at Cortland with a B.A. in international studies in 1990. In 1993 an M.S. in solid state physics was earned at Binghamton University, New York, with a thesis entitled "Magnetic Properties of Graphite bi-intercalation Compounds". Since then she has been working toward her Ph.D. in materials science and engineering with an emphasis on electronic materials at the University of Florida, Gainesville.

I certify that I have read this study and that in my opinion it conforms to acceptable standards of scholarly presentation and is fully adequate, in scope and quality, as a dissertation for the degree of Doctor of Philosophy.

Stephen J. Pearton, Chair
Professor of Materials Science
and Engineering

I certify that I have read this study and that in my opinion it conforms to acceptable standards of scholarly presentation and is fully adequate, in scope and quality, as a dissertation for the degree of Doctor of Philosophy.

Cammy R. Abernathy
Professor of Materials Science
and Engineering

I certify that I have read this study and that in my opinion it conforms to acceptable standards of scholarly presentation and is fully adequate, in scope and quality, as a dissertation for the degree of Doctor of Philosophy.

Joseph Simmons
Professor of Materials Science
and Engineering

I certify that I have read this study and that in my opinion it conforms to acceptable standards of scholarly presentation and is fully adequate, in scope and quality, as a dissertation for the degree of Doctor of Philosophy.

Jeff Childress
Assistant Professor Materials
Science and Engineering

I certify that I have read this study and that in my opinion it conforms to acceptable standards of scholarly presentation and is fully adequate, in scope and quality, as a dissertation for the degree of Doctor of Philosophy.

Fred Sharifi
Assistant Professor Physics

This dissertation was submitted to the Graduate Faculty of the College of Engineering and to the Graduate School and was accepted as partial fulfillment of the requirements for the degree of Doctor of Philosophy

December, 1996

Winfred M. Phillips
Dean, College of Engineering

Karen A. Holbrook
Dean, Graduate School